

# Variations in the D/H ratio of extended sightlines from *FUSE* observations<sup>1</sup>

Cristina M. Oliveira<sup>2</sup> and Guillaume Hébrard<sup>3</sup>

## ABSTRACT

We use new *FUSE* data to determine the column densities of interstellar D I, N I, O I, Fe II, and H<sub>2</sub> along the HD 41161 and HD 53975 sightlines. Together with  $N(\text{HI})$  from the literature (derived from *Copernicus* and *IUE* data) we derive D/H, N/H, and O/H ratios. These high column density sightlines have both  $\log N(\text{HI}) > 21.00$  and allow us to probe gas up to  $\sim 1300$  pc. In particular these sightlines allow us to determine the gas phase D/H ratio in a hydrogen column density range,  $\log N(\text{H}) > 20.70$ , where the only five measurements available in the literature yield a weighted average of  $\text{D}/\text{H} = (0.86 \pm 0.08) \times 10^{-5}$ . We find  $\text{D}/\text{H} = (2.14 \pm 0.51) \times 10^{-5}$  along the HD 41161 sightline. This ratio is  $\sim 3\sigma$  higher than the weighted mean D/H ratio quoted above, for sightlines with  $\log N(\text{H}) > 20.70$ , while the D/H ratio for the HD 53975 line of sight,  $\text{D}/\text{H} = (1.02 \pm 0.23) \times 10^{-5}$ , agrees within the  $1\sigma$  uncertainties. Our D/H measurement along the HD 41161 sightline presents the first evidence of variations of D/H at high  $N(\text{H})$ . Our result seems to indicate that either the long sightlines that according to the deuterium depletion model are dominated by cold undisturbed gas where deuterium would be depleted onto carbonaceous grains occur at higher  $N(\text{H})$  than previously thought or that the clumping of low D/H values in the literature for the long sightlines has another explanation. Another possibility to explain the high D/H toward HD 41161 is local production of D I which cannot be ruled out. Both of the O/H ratios derived here,  $(9.12 \pm 2.15) \times 10^{-4}$  and  $(5.37 \pm 1.35) \times 10^{-4}$  (for HD 41161 and HD 53975, respectively) are higher than what

---

<sup>1</sup>Based on observations made with the NASA-CNES-CSA *Far Ultraviolet Spectroscopic Explorer*. *FUSE* is operated for NASA by The Johns Hopkins University under NASA contract NAS5-32985.

<sup>2</sup>Department of Physics and Astronomy, The Johns Hopkins University, 3400 N. Charles St., Baltimore MD 21218

<sup>3</sup>Institut d'Astrophysique de Paris, 98 bis, Boulevard Arago, 75014 Paris, France.

has been found by other authors in studies containing many sightlines, although not inconsistent, in the case of HD 53975, with individual measurements along some sightlines. However, O/H along HD 41161 is extremely high, and together with other high O/H ratios based on *FUSE* data might indicate the presence of unknown systematic effects when deriving  $N(\text{OI})$  along high column density sightlines. Finally, we derive  $(\text{N}/\text{H}) \times 10^5 = 8.32 \pm \frac{2.09}{1.76}$  and  $5.07 \pm \frac{1.45}{1.21}$  and  $(\text{D}/\text{O}) \times 10^2 = 2.29 \pm \frac{0.40}{0.35}$  and  $1.91 \pm \frac{0.51}{0.43}$ , for HD 41161 and HD 53975, respectively. In addition, the relatively high signal-to-noise ratio of the HD 41161 data allows us to place constraints on the  $f$ -values of some neutral chlorine transitions, present in the *FUSE* bandpass, for which only theoretical values are available.

*Subject headings:* ISM: Abundances — ISM: Evolution — Ultraviolet: ISM — Stars: Individual (HD 41161, HD 53975)

## 1. INTRODUCTION

Deuterium is thought to be produced in appreciable amounts only in the Big Bang (Epstein et al. 1976). Of all the light elements produced during Big Bang Nucleosynthesis (e.g.,  $^3\text{He}$ ,  $^4\text{He}$ ,  $^7\text{Li}$ ), deuterium, easily destroyed in stellar interiors (astration), is the one whose relatively simple evolution makes it a particularly sensitive estimator of the baryonic density. Conversely, measurements of the cosmic microwave background, such as those performed with *WMAP* and other missions, can be used to infer the primordial abundance of deuterium,  $(\text{D}/\text{H})_{\text{P}}$ . Analysis of the three year *WMAP* data (Spergel et al. 2006) yields  $(\text{D}/\text{H})_{\text{P}}$  in agreement with that derived by Kirkman et al. (2003),  $(\text{D}/\text{H})_{\text{P}} = (2.78 \pm \frac{0.44}{0.38}) \times 10^{-5}$ , by taking the weighted average of five D/H measurements toward QSOs in the range  $z = 2.079$ – $3.572$ . Sembach et al. (2004) found  $\text{D}/\text{H} = (2.2 \pm 0.7) \times 10^{-5}$  for Complex C, a high-velocity low-metallicity cloud falling into our galaxy, which has presumably experienced more stellar processing than the gas seen toward QSOs.

Precise measurements of the gas-phase D/H ratio in the ISM were first performed with the *Copernicus* satellite (e.g., Rogerson & York 1973) followed by the *Hubble Space Telescope* twenty years later (*HST*, e.g., Linsky et al. 1995), IMAPS (Interstellar Medium Absorption Profile Spectrograph, Jenkins et al. 1999; Sonneborn et al. 2000), and more recently the *Far Ultraviolet Spectroscopic Explorer* (*FUSE*, e.g., Oliveira et al. 2006, and references therein). Variations in the D/H ratio were observed early on (York 1983) and by different satellites (e.g., Jenkins et al. 1999). Lemoine et al. (1999) discuss some of the mechanisms that could be responsible for the observed variations, based on the D/H data available at the time. However only after the launch of *FUSE* in 1999, has a large enough sample of sightlines

with differing D/H ratios been accumulated, allowing the question of what causes the D/H variations to be addressed in a more systematic way. While the constancy of the D/H ratio in the Local Bubble (LB, corresponding to  $\log N(\text{H}) \leq 19.2$ , Sfeir et al. 1999) seems to be a well accepted fact ( $(\text{D}/\text{H})_{\text{LB}} = (1.56 \pm 0.04) \times 10^{-5}$  from the compilation by Wood et al. 2004) two distinct explanations have emerged to explain the large scatter of gas-phase D/H measurements, in the Solar neighborhood outside of the LB. These measurements range from  $\text{D}/\text{H} = (0.50 \pm 0.16) \times 10^{-5}$  toward  $\theta$  Car derived by Allen et al. (1992) to  $\text{D}/\text{H} = (2.18 \pm_{0.19}^{0.22}) \times 10^{-5}$  toward  $\gamma^2$  Vel derived by Sonneborn et al. (2000).

Hébrard & Moos (2003) proposed a low value for the present-epoch deuterium abundance in the Solar neighborhood, based on indirect measurements of D/H from D/O and the constancy of the O/H ratio ( $\text{O}/\text{H} = (3.43 \pm 0.15) \times 10^{-4}$  from Meyer et al. 1998, updated  $f$ -value). Using more measurements than Hébrard & Moos (2003), Hébrard (2006) proposed then  $\text{D}/\text{H} = (0.7 \pm 0.2) \times 10^{-5}$  for the present-epoch deuterium abundance. The high D/H ratios observed would be due to unknown systematic errors in the determination of  $N(\text{H I})$ , unknown deuterium enrichment processes and/or local infall of deuterium-rich gas.

The possibility that deuterium could be depleted in dust grains was first proposed by Jura (1982). Draine (2004) and Draine (2006) explored further the theoretical plausibility of this process leading Wood et al. (2004) and Linsky et al. (2006) to propose that the depletion of deuterium into dust grains leads to different levels of depletion along sightlines with different histories, producing the observed scatter in D/H. In this scenario, the highest measurements of the gas-phase abundance of deuterium in the Solar neighborhood place a lower limit on the total deuterium abundance,  $\text{D}/\text{H} \geq (2.31 \pm 0.24) \times 10^{-5}$ , which one can then compare to the primordial value through chemical evolution models. Supporting evidence for this model includes correlations of D/H with the depletion of Ti (Prochaska et al. 2005), Fe and Si (Linsky et al. 2006), and with the average sightline density (Oliveira et al. 2006).

Galactic evolution models have to reproduce a number of observables such as the metallicity distribution of late type stars, along with predictions of the evolution of deuterium from its primordial value to its present day distribution in the Galaxy, and in particular its value in the Solar neighborhood. Romano et al. (2006) have addressed the different views on the behavior of the D/H ratio by considering what value of D/H is predicted for the Solar neighborhood by chemical evolution models that satisfy the majority of the observational constraints (such as the G-dwarf metallicity distribution). They find that a modest star formation and a continuous infall of unprocessed gas is required to fit all the observational data, leading only to a modest decrease of the deuterium abundance from its primordial value. According to the models of Romano et al. (2006), which adopt  $(\text{D}/\text{H})_{\text{P}} = 2.6 \times 10^{-5}$ ,

D/H in the Solar neighborhood should be in the range of  $(1.4\text{--}2.0)\times 10^{-5}$ , implying astration factors  $<1.8$ . Low D/H ratios, as the one proposed by Hébrard (2006) are ruled out because they produced significant disagreements with other observational constraints, in particular with the G-dwarf metallicity distribution.

Testing the two explanations above for the scatter in D/H, requires more measurements of D/H and other species that might yield information about the depletion and physical conditions along the sightlines, particularly along high column density sightlines. In this work we present analyses of the D/H and other ratios along the extended sightlines to HD 41161 and HD 53975. Both of these sightlines have total hydrogen column densities greater than  $10^{21} \text{ cm}^{-2}$ , and according to the variable deuterium depletion model such high column density sightlines should be biased by cold, not recently shocked gas, where deuterium would be depleted in grains. For the HD 53975 sightline we find  $D/H = (1.02 \pm_{0.20}^{0.23})\times 10^{-5}$ , a value slightly higher but comparable to those found previously for similar sightlines. The high D/H ratio along the HD 41161 sightline,  $D/H = (2.14 \pm_{0.43}^{0.51})\times 10^{-5}$ , presents the first evidence of D/H variations at high  $N(\text{H})$ , indicating that our understanding of the behavior of D/H is still incomplete.

This paper is organized as follows. The targets and their sightlines are presented in §2. §3 describes the observations and data processing, while §4 presents the analyses. The abundance of neutral hydrogen along the two sightlines is discussed in §5. The results are presented and discussed in §6. Constrains on the  $f$ -values of CII transitions present in the spectra of HD 41161 are derived in §7. Our work is summarized in §8. All uncertainties are quoted at the  $1\sigma$  level unless noted otherwise.

## 2. THE TARGETS AND THEIR SIGHTLINES

The properties of the two stars are listed in Table 1. Below we discuss each star in detail.

### 2.1. HD 41161

HD 41161 (O8V, Conti & Alschuler 1971) is a field star (Maíz-Apellániz et al. 2004) that probes gas in the direction  $l = 164.97^\circ$  and  $b = +12.89^\circ$  up to 1253 pc. Jenkins (1978) used *Copernicus* data to derive  $\log N(\text{O VI}) = 13.29$ . Using *IUE* data Shull & van Steenberg (1985) derived  $\log N(\text{HI}) = 20.98 \pm 0.07$ , while Diplas & Savage (1994a) determined  $\log N(\text{HI}) = 21.01 \pm 0.08$  also from *IUE* data. Taking into account these two determinations

of  $N(\text{HI})$  we adopt for the purpose of this study  $\log N(\text{HI}) = 21.00 \pm 0.09$ .

Dixon et al. (1998) determined the column densities of  $\text{H}_2$  ( $J = 0 - 5$ ) along this sightline using ORFEUS-1 data. The higher resolution and signal-to-noise of the *FUSE* data for HD 41161, allow us to determine  $\text{H}_2$  column densities with uncertainties smaller than the  $\sim 60\%$  (or more) quoted by Dixon et al. (1998).

## 2.2. HD 53975

HD 53975 (O7.5V, Conti & Alschuler 1971) is a spectroscopic binary (Garmany et al. 1980; Gies et al. 1994), member of the CMa OB1 association (Humphreys 1978) probing gas up to a distance of 1318 pc in the direction  $l = 225.68^\circ$  and  $b = -2.32^\circ$ . Based on observations obtained with *Copernicus*, Bohlin et al. (1978) determined  $\log N(\text{HI}) = 21.15 \pm {}_{0.10}^{0.08}$ . Shull & van Steenberg (1985) used *IUE* data to derive  $\log N(\text{HI}) = 21.11 \pm 0.08$ , while Diplas & Savage (1994a) determined  $\log N(\text{HI}) = 21.10 \pm 0.08$ , also from *IUE* data. We take the weighted average of the independent  $N(\text{HI})$  determinations based on *Copernicus* and *IUE* (Shull & van Steenberg 1985) data to adopt for this work  $\log N(\text{HI}) = 21.13 \pm 0.06$ .

## 3. OBSERVATIONS AND DATA PROCESSING

The *FUSE* observatory consists of four coaligned prime-focus telescopes and Rowland-circle spectrographs that produce spectra over the wavelength range 905 – 1187 Å, with a spectral resolution of  $\sim 15 - 20 \text{ km s}^{-1}$  (wavelength dependent) for point sources. Two of the optical channels employ SiC coatings, providing reflectivity in the wavelength range  $\sim 905 - 1000 \text{ Å}$ , while the other two have LiF coatings for maximum sensitivity above 1000 Å. Dispersed light is focused onto two photon-counting microchannel plate detectors. With this arrangement of optical channels (LiF 1, LiF 2, SiC 1, and SiC 2) and detector segments (1A, 1B, 2A, 2B) the *FUSE* instrument has 8 channels: LiF 1A, LiF 1B, LiF 2A, LiF 2B, SiC 1A, SiC 1B, SiC 2A, and SiC 2B. Four channels cover the wavelength range 1000 – 1080 Å while two channels each cover the ranges 900 – 1000 Å and 1080 – 1180 Å. Details about the *FUSE* mission, its planning, and on-orbit performance can be found in Moos et al. (2000) and Sahnou et al. (2000).

Table 2 summarizes the *FUSE* observations of HD 41161 and HD 53975. HD 41161 was observed by *FUSE* through the large (LWRS,  $30'' \times 30''$ ) and medium-sized (MDRS,  $4'' \times 20''$ ) apertures. During the short (58 s) LWRS observation data was obtained with the LiF and

SiC channels. During the longer (6520 s) MDRS observation only SiC data was obtained due to the flux of this star being very close to the *FUSE* bright object limit ( $10^{-10}$  erg s $^{-1}$  Å $^{-1}$  cm $^{-2}$ ). The lower reflectivity of the SiC channels compared to that of the LiF channels allows some bright targets to be observed, without damaging effects on the detectors.

The two-dimensional *FUSE* spectra are reduced using the CalFUSE pipeline v3<sup>1</sup>. The processing includes data screening for low quality or unreliable data, thermal drift correction, geometric distortion correction, heliocentric velocity correction, dead time correction, wavelength calibration, detection and removal of event bursts, background subtraction, and astigmatism correction. The spectra are aligned by cross-correlating the individual exposures over a short wavelength range that contains prominent spectral features and then coadded by weighting each exposure by its exposure time, using the CORRCAL software developed by S. Friedman.

The S/N of the LWRS data obtained for the HD 41161 sightline is inferior to that of the MDRS data. In our analysis we use SiC data from the MDRS observation (no LiF data was obtained during this observation) and only LiF data from the LWRS observation. The coadded MDRS data has a signal-to-noise ratio per pixel of 16.87 at  $\sim 918.5$  Å in the SiC 1B channel and of 32.7 at  $\sim 1032.2$  Å in the SiC 1A channel.

HD 53975 was observed by *FUSE* for 482 s through the MDRS aperture. Similarly to HD 41161 only SiC data were obtained during this observation due to the flux of this star being close to the *FUSE* bright object limit. We coadded the data for this target in the manner described above. The coadded data has a S/N per pixel of 10.25 at  $\sim 918.5$  Å in the SiC 1B channel and of 16.87 at  $\sim 1032.6$  Å in the SiC 1A channel.

Figure 1 and 2 present the *FUSE* spectra of the two targets.

#### 4. ANALYSIS

We use apparent optical depth, curve of growth, and profile fitting methods (AOD, COG, and PF, respectively) to determine column densities along the sight lines, whenever possible (see e.g. Oliveira et al. 2003, 2006, for further discussion of these methods). Details about the particular fitting routine used here (*Owens.f*) can be found in Hébrard et al. (2002) and Lemoine et al. (2002).

Table 3 lists the atomic data and equivalent widths of the transitions used in this study.

---

<sup>1</sup>The CalFUSE pipeline reference guide is available at [http://fuse.pha.jhu.edu/analysis/pipeline\\_reference.html](http://fuse.pha.jhu.edu/analysis/pipeline_reference.html)

A, C, and P are used to indicate which transitions are used with the AOD, COG, and PF techniques, respectively. No equivalent widths were measured for the transitions flagged only with 'P' due to blendings or in the case of DI because there are not enough unblended DI transitions to construct a curve-of-growth. These transitions were only used with the PF technique. We use the compilation by Morton (2003) for the atomic data and that of Abgrall et al. (1993a) and Abgrall et al. (1993b) for the molecular data.

#### 4.1. Atomic species along the line of sight to HD 41161

We use the AOD technique to place lower limits on the column densities of CI, CIII, NII, PII, ClII, and ArI along this sight line and to determine the column densities of DI, NI, FeII. With the COG method we derive column densities for NI, Fe II and  $b_{\text{NI}} = 8.3 \pm 0.2 \text{ km s}^{-1}$  and  $b_{\text{FeII}} = 9.2 \pm_{0.9}^{1.0} \text{ km s}^{-1}$ .

The PF technique is used in a similar manner in the analyses of both sightlines. We fit a single absorption component to the low ionization atomic species DI, NI, OI, and FeII, and another to the molecular species. HI is included in the fit as well, in a separate absorption component, with the sole purpose of modeling the continuum in the vicinity of the DI lines. We use a line spread function with a FWHM of  $0.0641 \text{ \AA}$  to fit the *FUSE* data, constant for all channels and wavelengths, corresponding to a spectral resolution of  $\sim 20 \text{ km s}^{-1}$  (see Williger et al. 2005, for a determination of the LSF across the *FUSE* bandpass and for a comparison between  $N$  obtained both with free and fixed LSFs). We derive a Doppler parameter  $b \sim 10 \text{ km s}^{-1}$  for the absorption component containing DI, NI, OI, and FeII, in agreement with  $b$  derived for NI and FeII with the COG technique. This Doppler parameter should not be viewed as the classic  $b$  composed of turbulent and thermal terms, but rather the result of line broadening due to multiple unresolved components along the sightline. Fits to some of the lines used with the PF method are presented in Figure 3.  $N(\text{DI})$  along this sightline is constrained mostly by the  $\lambda 916.2$  DI transition, which is free from blends with other lines, making  $N(\text{DI})$  independent of  $N(\text{H}_2)$ .

Table 4 presents the column densities of the atomic species obtained with the different methods as well as the adopted values. In this work we adopt values that are roughly at the midpoint of the values obtained with the different methods and uncertainties that include the extremes of the values obtained with the different methods. As a general rule we do not adopt  $1\sigma$  uncertainties smaller than  $0.05 \text{ dex}$  ( $\sim 12\%$ ) because we feel that adopting smaller uncertainties could be misleading, due to the presence of unknown systematic effects.

O VI is not clearly detected in our data. Using the  $\lambda 1032$  O VI transition we place a  $3\sigma$

upper limit on  $\log N(\text{OVI})$  of 13.0, while Jenkins (1978) determined  $\log N(\text{OVI}) = 13.29$  using *Copernicus* data. Since no uncertainties were quoted by Jenkins (1978) and given the S/N of the *Copernicus* data near the OVI  $\lambda 1032$  transition it is likely that the two determinations are compatible.

ClI is also detected along the HD 41161 sightline. We use the  $\lambda 1088$  ClI transition to determine  $N(\text{ClI})$  along this sight line with the AOD method. Besides the  $\lambda 1088$  transition, many other ClI transitions (for which only theoretically derived oscillator strengths are available) are detected. The high S/N ratio of the data allows us to place constraints on the  $f$ -values of several of these transitions. This is discussed in detail in § 7.

#### 4.2. H<sub>2</sub> and HD along the line of sight to HD 41161

Absorption by molecular hydrogen from the rotational levels  $J = 0$  through  $J = 5$  and by HD ( $J = 0$ ) is present in the spectra of HD 41161. We use the AOD technique to determine the column densities of HD ( $J = 0$ ) and H<sub>2</sub> ( $J = 4$  and  $J = 5$ ).

We fit a single- $b$  COG to the measured equivalent widths of HD and H<sub>2</sub> ( $J = 1$  through 5) for the HD 41161 sight line. Transitions from the rotational level  $J = 0$  are too blended with those of other species to allow measurements of equivalent widths. We determine  $b_{\text{H}_2} = 7.2 \pm_{0.2}^{0.4} \text{ km s}^{-1}$ .

We use the PF technique to determine the column densities of HD and H<sub>2</sub> along this sightline, by fitting one absorption component simultaneously, to multiple transitions of HD and H<sub>2</sub>. We derive  $b_{\text{H}_2} \sim 7 \text{ km s}^{-1}$ .

Table 5 presents the adopted molecular column densities along this sightline (following the same reasoning above, used to adopt the atomic column densities for this sightline). Our results agree with those derived by Dixon et al. (1998) except for  $J = 2$ , for which they quote  $\log N(J = 2) = 17.6 \pm 0.2$ , while we find  $\log N(J = 2) = 17.97 \pm 0.10$ . We find  $\log N(\text{H}_2) = 19.98 \pm 0.08$ . Using the column densities for the  $J = 0$  and  $J = 1$  levels we derive the excitation temperature  $T_{01} = 84 \pm 7 \text{ K}$ . This temperature is in good agreement with that found by Savage et al. (1977) from *Copernicus* observations of 61 sightlines with  $\log N(\text{H}_2) > 18.0$  ( $77 \pm 17 \text{ K}$ ) and that derived by Rachford et al. (2002) from a *FUSE* survey of sightlines with  $A_v \geq 1 \text{ mag}$  ( $68 \pm 15 \text{ K}$ ).

We derive  $\log N(\text{H}_2) = 19.98 \pm_{0.09}^{0.08}$ , which combined with  $N(\text{HI})$  from §2.1 leads to the total hydrogen column density along this sightline  $\log N(\text{H}) = \log (N(\text{HI}) + 2N(\text{H}_2)) = 21.08 \pm 0.08$ , and to the molecular fraction  $f_{\text{H}_2} = 2N(\text{H}_2)/N(\text{H}) = (16.0 \pm_{3.4}^{4.9}) \%$ .



### 4.3. Atomic species along the line of sight to HD 53975

The AOD technique is used to place lower limits on the column densities of C I, C III, N II, P II, S III, and Ar I and to determine column densities of D I, N I, O VI, Fe II, and Cl I along the HD 53975 sight line.

We use the COG method to derive column densities of N I and Fe II along the HD 53975 sightline. We derive  $b_{\text{N I}} = 9.6 \pm 0.4 \text{ km s}^{-1}$  and  $b_{\text{Fe II}} \sim 12 \text{ km s}^{-1}$ .

With the PF technique we fit a single absorption component to the low ionization atomic species D I, N I, O I, Fe II, and Mg II, and another to the molecular species. H I is included in the fit as well, in a separate absorption component, with the sole purpose of modeling the continuum in the vicinity of the D I lines. A separate component is used to model the absorption by O VI. We use a line spread function with a FWHM of  $0.0641 \text{ \AA}$  to fit the *FUSE* data, constant for all channels and wavelengths, corresponding to a spectral resolution of  $\sim 20 \text{ km s}^{-1}$ . Figure 4 presents fits to some of the lines used to determine the column densities along this sightline. We derive  $b \sim 15 \text{ km s}^{-1}$  for the absorption component containing D I. Similarly to HD 41161, this Doppler parameter reflects the broadening of the lines due to multiple unresolved absorption components along the line of sight. From the 4 D I transitions used to constrain  $N(\text{D I})$  (see Table 3) only the  $\lambda 916.9$  line suffers from major blends with  $\text{H}_2$  ( $J = 3$ ) whose column density is not well constrained (see § 4.4 below). Removing this D I line from the fits does not affect  $N(\text{D I})$  adopted. Table 6 presents the atomic column densities along this sightline obtained with the different methods as well as the adopted values (see § 4.1 for how values and uncertainties are adopted).

### 4.4. $\text{H}_2$ and HD along the line of sight to HD 53975

Absorption by HD and by molecular hydrogen from the rotational levels  $J = 0$  through  $J = 5$  is detected along this sightline. We use the AOD technique to determine the column densities of the  $\text{H}_2$   $J = 4$  and  $J = 5$  levels.

Similarly to HD 41161 we fit a single- $b$  COG to the measured equivalent widths of  $\text{H}_2$  ( $J = 0$  through 5) and we use the PF method to determine the column densities of the different  $\text{H}_2$   $J$  levels and HD by fitting one absorption component to  $\text{H}_2$  and HD. We find that the column densities of the levels  $J = 0$  through  $J = 3$  derived with the COG method are at least a factor of  $\sim 2$  larger than the ones derived with the PF technique. An  $\text{H}_2$  absorption model containing the column densities and Doppler parameter derived with the single- $b$  COG leads to  $\text{H}_2$  absorption profiles that are inconsistent with the data and that clearly overestimate the true  $N(\text{H}_2)$  along this sightline. For this reason we adopt for  $N(\text{H}_2)$  along this sightline

the results derived with the AOD and PF techniques. Transitions from the  $J = 2$  and  $J = 3$  rotational levels are on the flat part of the curve of growth, hence the associated column densities are very uncertain and are flagged with ‘?’ in Table 5.

We note that  $N(\text{DI})$  is not affected by the adopted  $N(\text{H}_2)$  as fits performed where the DI lines blended with  $\text{H}_2$  were removed from the fit (particularly  $\lambda 916.9$ ) lead to  $N(\text{DI})$  consistent with the value adopted in Table 6.

Table 5 presents the adopted molecular column densities for this sightline (see § 4.1 for how values and uncertainties are adopted). We find  $\log N(\text{H}_2) = 19.18 \pm 0.04$  by adding the column densities of the  $J = 0$  and  $J = 1$  levels, which contain most of the  $\text{H}_2$  along this sightline. Using the column densities for these two levels we derive the excitation temperature  $T_{01} = 93 \pm 9$  K, in agreement with that found by Savage et al. (1977) but slightly higher than that found by Rachford et al. (2002). The total hydrogen column density along this sightline is then  $N(\text{H}) = 21.14 \pm 0.06$  with  $f_{\text{H}_2} = (2.2 \pm_{0.3}^{0.4})\%$ .

## 5. NEUTRAL HYDROGEN ABUNDANCES

### 5.1. $N(\text{HI})$ ALONG THE HD 41161 LINE OF SIGHT

To check the consistency of  $N(\text{HI})$  determined from the  $\text{Ly}\alpha$  transition in the *IUE* data, we use some of the HI Lyman transitions in the *FUSE* bandpass to determine  $N(\text{HI})$ , with the profile fitting technique. The following transitions are used to constrain  $N(\text{HI})$ :  $\lambda\lambda$  1025, 972, 920, 918, 917, and 916. No stellar model is used in conjunction with the *FUSE* data. We fit an absorption model with one component of  $\text{H}_2$ , one component containing DI, OI, FeII, and ArI, and another component with HI. The damped wings of the  $\text{Ly}\beta$  transition constrain  $N(\text{HI})$ , while the weaker Lyman lines constrain  $b_{\text{HI}}$ . In addition to fitting the Lyman lines we include also other regions of the spectra containing absorption lines of  $\text{H}_2$  and other atomic species, to constrain the shapes of absorption lines of these species that are unresolved from the HI Lyman transitions. Figure 5 presents the fit to the  $\text{Ly}\beta$  and  $\text{Ly}\gamma$  HI transitions along the HD 41161 sight line. The fit yields  $\log N(\text{HI}) = 21.13 \pm_{0.05}^{0.04}$  and  $b_{\text{HI}} \sim 14 \text{ km s}^{-1}$ , in reasonable agreement with  $\log N(\text{HI}) = 21.00 \pm 0.09$  adopted (see §2.1). Varying the degree of the polynomials used to define the continua for the  $\text{Ly}\beta$  and  $\text{Ly}\gamma$  transitions leads to  $\log N(\text{HI})$  in agreement with  $21.13 \pm_{0.05}^{0.04}$ .

## 5.2. $N(\text{HI})$ ALONG THE HD 53975 LINE OF SIGHT

Similarly to HD 41161, we check the consistency of  $N(\text{HI})$  derived from the *IUE* and *Copernicus* data by fitting some of the Ly HI transitions in the *FUSE* bandpass. We fit an absorption model with one component of  $\text{H}_2$ , a second component with D I, N I, O I, and Fe II, and a third component containing HI. The following HI Lyman lines are used to constrain  $N(\text{HI})$ :  $\lambda\lambda$  916.4, 917.2, 919.3, 920.9, 972, and 1025. Figure 6 presents the resulting fits to the HI Ly $\beta$  and Ly $\gamma$  transitions. We derive  $\log N(\text{HI}) = 21.19 \pm 0.01$  (formal statistical errors) and  $b_{\text{HI}} \sim 15 \text{ km s}^{-1}$ , in agreement with the adopted value  $\log N(\text{HI}) = 21.13 \pm 0.06$ .

## 6. RESULTS AND DISCUSSION

Table 7 summarizes several ratios along the two sightlines. Below we discuss each ratio in detail.

### 6.1. D/H ratios

In the discussion below the D/H ratios are determined using  $\text{D/H} = [N(\text{D}) + N(\text{HD})]/[N(\text{HI}) + 2 \times N(\text{H}_2) + N(\text{HD})]$ .

#### 6.1.1. D/H along the HD 41161 sightline

Figure 7 presents the D/H ratio as a function of  $\log N(\text{H})$ . Open squares represent values from the literature and the three new values from Oliveira et al. (2006) (references for all the ratios can be found in this paper), filled circles the ratios derived in this work. The Local Bubble D/H ratio and uncertainties are represented by horizontal solid and dashed lines. The vertical dashed line at  $\log N(\text{H}) = 19.2$  represents the edge of the Local Bubble, while the vertical dashed line at  $\log N(\text{H}) = 20.7$  represents the approximate position of where a new low and constant D/H regime was proposed to exist by Wood et al. (2004) and Linsky et al. (2006).

There are five sight lines with  $\log N(\text{H}) > 20.7$ , with D/H ratios available in the literature (HD 198965, HD 191877, JL 9, LS 1274, and HD 90087; Hoopes et al. 2003; Wood et al. 2004; Hébrard et al. 2005). For these sightlines with  $20.7 < \log N(\text{H}) < 21.20$ , the weighted mean is  $\text{D/H} = (0.86 \pm 0.08) \times 10^{-5}$ . HD 41161 has  $N(\text{H})$  similar to these sightlines, but a D/H

ratio inconsistent by  $\sim 3\sigma$ . To make D/H along the HD 41161 sightline consistent with the weighted ratio of the other 5 sightlines, one would have to increase  $N(\text{H})$  by a factor of  $\sim 2.49$ , or  $\log N(\text{HI})$  from 21.00 to  $\sim 21.44$ . To test whether D/H along this sightline could be high due to  $N(\text{HI})$  being underestimated we performed fits where  $\log N(\text{HI})$  was forced to 21.44. Figure 8 presents the fits to HI Ly $\beta$  and Ly $\gamma$  with  $\log N(\text{HI})$  forced to 21.44. The degree of the polynomial used to fit the continuum of these two transitions, is the same as the one used for the fit where we determined  $N(\text{HI}) = 21.13 \pm \begin{smallmatrix} 0.04 \\ 0.05 \end{smallmatrix}$ . However, in this case, the continuum is forced to be artificially high to accommodate the higher  $N(\text{HI})$ . In addition, the fit grossly overestimates the absorption on the blue side of the core of the Ly lines as shown in the two bottom panels of Figure 8. To further check that  $\log N(\text{HI}) = 21.44$  overestimates the true HI absorption we retrieved the *IUE* Ly $\alpha$  spectrum for the HD 41161 sightline from the MAST archive (no further processing was applied). Figure 9 presents the fit to HI Ly $\alpha$  forcing  $\log N(\text{HI}) = 21.44$ . Similarly to the fits to Ly $\beta$  and Ly $\gamma$  discussed above, forcing such a high value of  $N(\text{HI})$  on the data forces the continuum to be artificially high and overestimates the absorption near the core of the Ly $\alpha$  line.

The  $N(\text{HI})$  adopted for this sightline is based on measurements performed by two different sets of authors (Shull & van Steenberg 1982; Diplas & Savage 1994b) who obtain similar results, although both used the same *IUE* dataset. In addition, fits of the Ly $\beta$  and Ly $\gamma$  HI transitions produce  $N(\text{HI})$  in agreement with the value adopted in §2.1, while forcing  $N(\text{HI})$  to the value required to bring D/H to agree with the other low D/H measurements in the literature (discussed above) produces fits that clearly overestimate the HI absorption. We conclude then that the high D/H along this sightline is unlikely due to  $N(\text{HI})$  being underestimated.

Another possibility to explain the high D/H along this sightline is that  $N(\text{DI})$  is overestimated. This is probably unlikely since saturation tends to move column densities in the opposite direction, i.e., underestimation rather than overestimation. However other factors, such as continuum placement, could produce the desired effect. A DI column density of  $\log N(\text{DI}) = 16.00$  is required to bring D/H along this sightline down to the weighted mean derived by the 5 sightlines discussed above. To test whether this  $N(\text{DI})$  value is consistent with the data we consider the  $\lambda 916.18$  and  $\lambda 919.1$  DI transitions. With the AOD method we derive  $\log N(\text{DI}) = 16.37 \pm 0.04$  from the  $\lambda 916.2$  transition and our fits yield  $\log N(\text{DI}) = 16.43 \pm 0.03$ . A column density of  $\log N(\text{DI}) = 16.0$  clearly underestimates the true DI absorption, as shown in Figure 10 where we overplot the above column density on the  $\lambda 916.2$  transition.

To further check our  $N(\text{DI})$  measurement along this sightline we can consider the  $\lambda 919.1$  DI transition. This transition, not used in our analysis of this sightline, is blended with H $_2$  ( $J$

= 4) and according to our model slightly saturated. Using our H<sub>2</sub> fit model we carefully deblend the DI and H<sub>2</sub> transitions. We use then the AOD technique to derive a lower limit to  $N(\text{DI})$  using the deblended DI  $\lambda 919.1$  transition. This exercise yields  $\log N(\text{DI}) > 16.13$ , indicating that it is unlikely that  $N(\text{DI})$  is overestimated.

We conclude then that the high D/H ratio along this sightline is unlikely due to either underestimation or overestimation of the HI or DI column densities, respectively.

According to the variable deuterium depletion model proposed by Linsky et al. (2006), sightlines that probe gas with high column densities should be biased by cold, not recently shocked gas, where deuterium would be depleted in grains. The high D/H toward HD 41161 might indicate that this scenario occurs at  $N(\text{H})$  higher than what was previously thought or that the clumping of low D/H values in the literature has another explanation. There is also the possibility that this sightline is dominated by gas which has been shocked and where the typical traces of a shock, such as highly ionized species (not detected along this sightline), have been erased. In this scenario the timescale to erase the traces of the shock would have to be smaller than that for D to deplete into the grains. The presence of cold H<sub>2</sub> ( $T_{01} = 84 \pm 7$  K) along this sightline does not necessarily imply that the gas is cold and undisturbed since H<sub>2</sub> is only a minor constituent of the sightline. Finally, we cannot rule out that local production of DI of the type proposed by Mullan & Linsky (1999) or Prodanović & Fields (2003) is responsible for all or part of the deuterium enhancement along this sightline.

To determine the iron depletion along this sightline,  $D(\text{Fe}) = \text{Log} (\text{Fe}/\text{H})_{\text{gas}} - \text{Log} (\text{Fe}/\text{H})_{\odot}$ , we use the solar abundance ratio  $\text{Log} (\text{Fe}/\text{H})_{\odot} = -4.55 \pm 0.05$  from Asplund et al. (2005). We find for this sightline,  $D(\text{Fe}) = -1.55 \pm 0.11$ . In a manner similar to some other sightlines with high D/H ratios, the Fe/H ratio along this sightline does not fit the trend of high Fe/H versus high D/H, displayed for most of the cases shown in Figure 3 of Linsky et al. (2006). There are however a few sightlines in Figure 3 of the paper mentioned above that seem to follow a trend different than most of the points, in that for the same Fe depletion a higher D/H ratio is found. The D/H and Fe/H ratios along the sightline to HD 41161 seem to follow this trend as well. Linsky et al. (2006) discuss some of the reasons that could lead to this sort of behavior and argue that these sightlines could either contain a smaller percentage of carbon grains (thus fewer sites for deuterium to deplete) or could have had weak shocks pass by which would have evaporated deuterium from the grain mantles.

### 6.1.2. *D/H along the HD 53975 sightline*

For the HD 53975 sightline we derive  $D/H = (1.02 \pm_{0.20}^{0.23}) \times 10^{-5}$  in agreement with the weighted mean  $D/H = (0.86 \pm 0.08) \times 10^{-5}$ , quoted above. Although the  $D/H$  ratio along the HD 41161 sightline indicates that  $D/H$  is variable for  $\log N(\text{H}) > 20.7$ , the  $D/H$  ratio along the HD 53975 sightline follows the trend displayed by the other other five sightlines in the literature with  $\log N(\text{H}) > 20.7$ . Taking into account this ratio, along with the ratios for the five sightlines mentioned above, yields a weighted mean  $D/H = (0.89 \pm 0.07) \times 10^{-5}$  (with  $\chi^2_\nu = 0.4$  for 5 degrees of freedom; the average of the upper and lower  $1\sigma$  uncertainties of individual ratios are used to determine weighted means in this work). The iron depletion along this sightline,  $D(\text{Fe}) = -1.75 \pm 0.09$ , follows the trend of low  $\text{Fe}/\text{H}$  versus low  $D/H$  displayed in Figure 3 of Linsky et al. (2006).

## 6.2. O/H Ratios

The O/H ratio along the HD 41161 sightline,  $\text{O}/\text{H} = (9.12 \pm_{1.83}^{2.15}) \times 10^{-4}$ , is more than  $3\sigma$  away from  $\text{O}/\text{H} = (3.43 \pm 0.15) \times 10^{-4}$  derived for 13 lines of sight probing gas within 1500 pc (most within 500 pc), with  $20.18 \leq \log N(\text{HI}) \leq 21.28$  by Meyer et al. (1998) (updated  $f$ -value). For HD 53975,  $\text{O}/\text{H} = (5.37 \pm_{1.14}^{1.35}) \times 10^{-4}$ , is  $\sim 1.7\sigma$  away from the Meyer et al. (1998) O/H ratio. The *FUSE*-based O/H measurements present a larger scatter than those based on *HST* data (see for example André et al. 2003; Cartledge et al. 2004). Figure 11 presents a compilation of O/H measurements performed with *FUSE* (from this work and the compilation by Oliveira et al. 2006, asterisks and filled circles, respectively) and *HST* data (from Cartledge et al. 2004, diamonds). For the *FUSE* measurements we consider only sightlines that probe gas beyond the Local Bubble, i. e.,  $\log N(\text{H}) > 19.2$ , since previous measurements by Oliveira et al. (2005) have shown that  $\text{O}/\text{H} = (3.45 \pm 0.19) \times 10^{-4}$  in the LB. The assumption that all the *HST* O/H measurements can be described by a single mean leads to the weighted mean  $\text{O}/\text{H} = (3.51 \pm 0.10) \times 10^{-4}$  with  $\chi^2_\nu = 1.35$  for 51 degrees of freedom. Assuming that the *FUSE* measurements can also be described by a single mean leads to the weighted mean  $\text{O}/\text{H} = (3.56 \pm 0.13) \times 10^{-4}$  but with  $\chi^2_\nu = 5.4$  for 18 degrees of freedom. The scatter in the *FUSE* O/H measurements is more pronounced in the range  $20.0 \leq \text{Log } N(\text{H}) \leq 20.9$ , where there are only a few *HST* measurements available. Hence, the scatter in the *FUSE* measurements might be due to there really being more scatter for lower column density sightlines, even if the O/H values for the LB show little scatter (Oliveira et al. 2005).

The larger (than Meyer et al. 1998) sample of sightlines probed by the work of Cartledge et al. (2004) contains some sightlines with O/H ratios  $\sim 6 \times 10^{-4}$ . For example, HD 91824

( $l = 285.70^\circ$ ,  $b = 0.07^\circ$ ) and HD 91983 ( $l = 285.88^\circ$ ,  $b = 0.05^\circ$ ) are both members of the Carina OB1 association (located at  $d \sim 2.5$  kpc) and have  $O/H = (6.91 \pm \frac{1.21}{0.92}) \times 10^{-4}$  and  $(5.25 \pm \frac{1.21}{0.98}) \times 10^{-4}$ , respectively (Cartledge et al. 2004, based on *HST* data). HD 90087 ( $l = 285.16^\circ$ ,  $b = -2.13^\circ$ ) is also part of the Carina OB1 association and is  $\sim 100$  pc away from the two other stars. For this sightline the *FUSE* derived  $O/H = (5.8 \pm 1.0) \times 10^{-4}$  (Hébrard et al. 2005) is in good agreement with the  $O/H$  ratios derived for the other members of this association.

In view of the Cartledge et al. (2004) measurements, the  $O/H$  ratio along the HD 53975 sightline does not seem to abnormally high, however the ratio along the line of sight to HD 41161 does.  $N(OI)$  is determined using the only unsaturated  $OI$  transition in the *FUSE* bandpass,  $\lambda 974$ , which is heavily blended with  $H_2$   $J = 2$  and  $J = 5$ . One might suspect that an erroneous  $f$ -value would lead to an inaccurate  $N(OI)$ . However, previous studies by Hébrard et al. (2005) indicate that  $N(OI)$  derived from this transition is consistent with  $N(OI)$  derived both from weaker and stronger  $OI$  transitions. Unknown blends with stellar lines are also the unlikely cause of a seemingly high  $N(OI)$  due to the high  $v_{\text{ sini}}$  of HD 41161. We suspect that unknown systematic effects when deriving  $N(OI)$  from the heavily blended  $\lambda 974$   $OI$  transition might be responsible for at least part of the scatter in the *FUSE* based  $O/H$  measurements.

### 6.3. N/H, O/N, and D/O Ratios

We derive  $N/H = (8.32 \pm \frac{2.09}{1.76}) \times 10^{-5}$  and  $N/H = (5.07 \pm \frac{1.45}{1.21}) \times 10^{-5}$  for the HD 41161 and HD 53975 sightlines, respectively. The first ratio is consistent, within the uncertainties, with  $N/H = (7.5 \pm 0.4) \times 10^{-5}$  derived by Meyer et al. (1997). The  $N/H$  ratio for the HD 53975 sightline is  $\sim 1.7\sigma$  away from the Meyer et al. (1997).

We derive  $O/N = 10.96 \pm \frac{2.10}{1.85}$  and  $O/N = 11.74 \pm \frac{3.36}{2.80}$  along the HD 41161 and HD 53975 sightlines, respectively. The  $O/N$  ratios for HD 41161 and HD 53975 are more than  $3\sigma$  and  $2.7\sigma$ , respectively, away from  $O/N = 4.1 \pm 0.3$  derived using the values of  $O/H$  and  $N/H$  determined by Meyer et al. (1998) and Meyer et al. (1997). This is likely a consequence of the high  $O/H$  for the two sightlines, in addition to the low  $N/H$  for the HD 53975 sightline.

We derive  $D/O = (2.29 \pm \frac{0.40}{0.35}) \times 10^{-2}$  and  $D/O = (1.91 \pm \frac{0.51}{0.43}) \times 10^{-2}$  along the HD 41161 and HD 53975 sightlines, respectively. Both of these ratios are consistent within the uncertainties with the weighted average  $D/O = (1.75 \pm 0.18) \times 10^{-2}$  derived by Hébrard et al. (2005) for the distant sightlines. The low dispersion of  $D/O$  at high  $N(H)$  has been used by Hébrard & Moos (2003) and Hébrard (2006) as an argument against a high  $D/H$  ratio being

representative of the interstellar medium in the Solar neighborhood. However, as pointed out above, the large scatter in the *FUSE* derived O/H ratios seems to indicate that  $N(\text{OI})$  might suffer from unknown systematic errors, which would affect the derived D/O ratios. If the high value of  $N(\text{OI})$  measured along the HD 41161 sightline is indeed too high due to systematic effects related to using the  $\lambda 974$  transition, then the D/O ratio along this sightline would have to be revised upwards becoming inconsistent with the Hébrard et al. (2005) D/O ratio for distant sightlines. This would be consistent with our claim, from D/H, that the deuterium abundance towards HD 41161 is higher than that along the other  $\log N(\text{H}) > 20.7$  sightlines.

Finally, we would like to point out that there are other sightlines in which high D/H, low D/O, and high O/H ratios are also observed, similarly to the HD 41161 sightline. These are Feige 110 (Friedman et al. 2002; Hébrard et al. 2005), PG 0038+199 (Williger et al. 2005), and LSE 44 (Friedman et al. 2006). Discussions about the possible causes of these ratios are given in the papers quoted for each sightline.

## 7. $f$ -VALUES OF CHLORINE

Chlorine has a unique chemistry, in which it can react exothermically with molecular hydrogen. Chlorine is ionized in regions where hydrogen is mostly in the atomic form, whereas in regions where there is a significant amount of molecular hydrogen, chlorine is mostly neutral with a small fraction in the HCl molecular form (Jura 1974; Jura & York 1978). Cl I traces then the cold molecular components along the sight lines. Determining accurate Cl I column densities requires accurate oscillator strengths; however only a few transitions have experimentally determined  $f$ -values. The *FUSE* bandpass contains numerous transitions of Cl I, many of which are detected along the HD 41161 sight line. In addition, the strong  $\lambda 1347$  Cl I transition is also detected in the *IUE* data for this star. Schectman et al. (1993) determined the  $f$ -values of several Cl I transitions using beam-foil spectroscopy. While the  $f$ -value of Cl I  $\lambda 1347$  had been previously measured experimentally,  $\lambda \lambda 1088, 1097$  had only theoretically determined  $f$ -values. The work by Schectman et al. (1993) presents then the first and only up to now, experimental measurement of the  $f$ -values of the  $\lambda 1088$ , and  $\lambda 1097$  transitions, and the most accurate measurement of the  $f$ -value of  $\lambda 1347$ .

Using two Cl I transitions which have experimentally determined  $f$ -values ( $\lambda \lambda 1088, 1347$ ) we place constraints on the  $f$ -values of other transitions whose currently adopted theoretical  $f$ -values (see Morton 2003, and references therein) are obviously incorrect. For two transitions that are optically thin, i. e., on the linear part of the COG, one can derive the relationship between their equivalent widths,  $W_{\lambda_1}/W_{\lambda_2} = (f_1 \times \lambda_1^2)/(f_2 \times \lambda_2^2)$ . We can then use



the wavelengths and experimentally derived  $f$ -values (as well as their associated uncertainties) for the  $\lambda 1088$  and  $\lambda 1347$  ClI transitions to derive the predicted ratio  $(W_{1347}/W_{1088})_{\text{pred}}$ . Table 8 presents the atomic data and equivalent widths of the ClI transitions detected along the HD 41161 sight line as well as  $1 \sigma$  upper limits on the equivalent widths of non-detected transitions. The fourth column in the table lists the references for the  $f$ -values. Using the data on this table we derive  $(W_{1347}/W_{1088})_{\text{pred}} = 2.90 \pm 0.33$ , under the assumption that for the HD 41161 sightline these two transitions lie in the linear part of the COG. Using the measured equivalent widths and their uncertainties from Table 8 for these two transitions we derive  $(W_{1347}/W_{1088})_{\text{meas}} = 2.35 \pm 0.41$ . The agreement between the predicted and measured equivalent width ratios indicates that the linear COG assumption is a valid approximation for this sightline. Since ClI traces the cooler components of a cloud, where hydrogen is mostly in molecular form, it is possible that there are more than one ClI components, not resolved by *FUSE*. However, as shown by Jenkins (1986), there are cases in which the combined equivalent widths of a population of Gaussian-like interstellar absorption components exhibit a COG which closely mimics that of a single, pure Gaussian distribution in velocity.

Although it seems that the approach above is valid for this sight line we take a conservative viewpoint by assuming that ClI  $\lambda 1347$  could be mildly saturated, but that ClI  $\lambda 1088$  is not. We use then the equivalent width of this transition as well as its uncertainty to predict the  $f$ -values of the other weaker ClI transitions quoted in Table 8 using the laboratory measured  $f_{1088}$  and its uncertainty. For the transition  $x$  the predicted  $f_x$  is then  $f_x = f_{1088} \times (W_x/W_{1088}) \times (\lambda_{1088}/\lambda_x)^2$ . Blending of ClI lines with stellar lines is not a concern for this sightline due to the high  $v_{\text{ sini}}$  of this star (see Table 1). In addition, careful modeling of the  $\text{H}_2$  and HD absorption along this sight line assures us that the ClI lines studied here are free from blends with these molecular species. In particular, the  $\lambda 1088$  ClI transition which falls near a CO transition ( $\lambda 1087.868$ ) is not affected by a blend with this molecular species as  $\log N(\text{CO}) < 13.5$  along this sightline. The last column in Table 8 presents the predicted  $f$ -values (and  $1 \sigma$  uncertainties), using the equation above, which can then be compared to the  $f$ -values from the literature quoted in the second column of this table.

Our results, presented in the last column of Table 8, indicate that some ClI transitions need to have their  $f$ -values revised by large factors. For instance, the currently used  $f$ -value for  $\lambda 1085$  is underestimated by a factor of  $\sim 38$ , while that for  $\lambda 1031$  is overestimated by a factor of  $\sim 7$ . While the aim of this work is not to determine empirically the ClI  $f$ -values in the *FUSE* bandpass, the set of revised  $f$ -values we present in Table 8 should provide a better match to the observations and can be used in the future for comparison with new theoretical calculations. For a comprehensive study of the oscillator strengths of many ClI transitions, including several not covered here, we direct the reader to the work by Sonnentrucker et al. (2006, in preparation).

Taking into account the uncertainties in the  $f$ -value of 1088 as well as on the measured equivalent width and assuming that this transition is on the linear COG we derive  $\log N(\text{ClI}) = 13.72 \pm 0.04$ .

There is a weak absorption feature around  $976 \text{ \AA}$  ( $W_\lambda = 19.5 \pm 1.6 \text{ \AA}$ ) which we suspect to be from chlorine, as we have not been able to identify it with other lines of other atomic or molecular species. We use the  $\text{H}_2$  ( $J = 2$ )  $\lambda 975.3507$  and HD ( $J = 0$ )  $\lambda 975.5821$  lines to derive the wavelength of this unknown transition by assuming that it traces the same absorption component as  $\text{H}_2$  and HD. The *FUSE* wavelength solution is expected to be accurate to about  $6 \text{ km s}^{-1}$  which at these wavelengths translates into  $\sim 0.02 \text{ \AA}$ . We derive then  $\lambda = 976.17 \text{ \AA}$  for this unknown transition.

## 8. SUMMARY

We have used *FUSE* data to determine the abundance of several atomic and molecular species along the sightlines to HD 41161 and HD 53975. Together with  $N(\text{HI})$  from the literature, we derive D/H, N/H, O/H, and D/O ratios for these sightlines. We find that while the D/H ratio along the HD 53975 sightline is consistent with five previous measurements at similar  $N(\text{H})$ , the ratio toward HD 41161 is surprisingly high and presents the first evidence of D/H variations for sightlines with high  $N(\text{H})$ . The pattern of low D/H for sightlines with large  $N(\text{H})$ , pointed out by Hébrard & Moos (2003) and emphasized by Wood et al. (2004) and Hébrard et al. (2005) is based on a small number of sightlines. Taking into account that at this high  $N(\text{H})$  there is a selection bias against high D/H measurements (Oliveira et al. 2006) it is not surprising that only 1 out of 7 sightlines present high D/H ratios. As analyses of D/H along other high column density sightlines are being performed, one might expect that future measurements will also produce high D/H ratios, indicating that our understanding of the mechanisms responsible for the observed D/H pattern are still incomplete. Finally, the large number of ClI transitions detected in the spectra of HD 41161 allows to place significant constraints on the  $f$ -values of several transitions for which only theoretical values are available.

This work is based on data obtained for the Guaranteed Time Team by the NASA-CNES-CSA *FUSE* mission operated by The Johns Hopkins University. Financial support to U. S. participants has been provided in part by NASA contract NAS5-32985 to Johns Hopkins University. Financial support to G. Hébrard has been provided by CNES. Based on observations made with the *International Ultraviolet Explorer*, obtained from the Data Archive at the Space Telescope Science Institute, which is operated by the Association of

Universities for Research in Astronomy, Inc. under NASA contract NAS5-26555. Support for MAST for non-HST data is provided by the NASA Office of Space Science via grant NAG5-7584 and by other grants and contracts. The profile fitting procedure, Owens.f, used in this work was developed by M. Lemoine and the French *FUSE* Team.

## REFERENCES

- Abgrall, H., Roueff, E., Launay, F., Roncin, J. Y., & Subtil, J. L. 1993a, *A&AS*, 101, 273  
— . 1993b, *A&AS*, 101, 323
- Allen, M. M., Jenkins, E. B., & Snow, T. P. 1992, *ApJS*, 83, 261
- André, M. K., Oliveira, C. M., Howk, J. C., Ferlet, R., Désert, J.-M., Hébrard, G., Lacour, S., des Étangs, A. L., Vidal-Madjar, A., & Moos, H. W. 2003, *ApJ*, 591, 1000
- Asplund, M., Grevesse, N., & Sauval, A. J. 2005, in *ASP Conf. Ser. 336: Cosmic Abundances as Records of Stellar Evolution and Nucleosynthesis*, ed. T. G. Barnes, III & F. N. Bash, 25–+
- Biemont, E., Gebarowski, R., & Zeippen, C. J. 1994, *A&A*, 287, 290
- Bohlin, R. C., Savage, B. D., & Drake, J. F. 1978, *ApJ*, 224, 132
- Cartledge, S. I. B., Lauroesch, J. T., Meyer, D. M., & Sofia, U. J. 2004, *ApJ*, 613, 1037
- Conti, P. S. & Alschuler, W. R. 1971, *ApJ*, 170, 325
- Diplas, A. & Savage, B. D. 1994a, *ApJS*, 93, 211  
— . 1994b, *ApJ*, 427, 274
- Dixon, W. V. D., Hurwitz, M., & Bowyer, S. 1998, *ApJ*, 492, 569
- Draine, B. T. 2004, *Bulletin of the American Astronomical Society*, 36, 1436
- Draine, B. T. 2006, in *Astronomical Society of the Pacific Conference Series*, ed. G. Sonneborn, H. W. Moos, & B.-G. Andersson, 58–+
- Epstein, R. I., Lattimer, J. M., & Schramm, D. N. 1976, *Nature*, 263, 198
- Friedman, S. D., Hébrard, G., Tripp, T. M., Chayer, P., & Sembach, K. R. 2006, *ApJ*, 638, 847

- Friedman, S. D., Howk, J. C., Chayer, P., Tripp, T. M., Hébrard, G., André, M., Oliveira, C., Jenkins, E. B., Moos, H. W., Oegerle, W. R., Sonneborn, G., Lamontagne, R., Sembach, K. R., & Vidal-Madjar, A. 2002, *ApJS*, 140, 37
- Garmany, C. D., Conti, P. S., & Massey, P. 1980, *ApJ*, 242, 1063
- Gies, D. R., Fullerton, A. W., Bolton, C. T., Bagnuolo, Jr., W. G., Hahula, M. E., & Wiemker, R. 1994, *ApJ*, 422, 823
- Hébrard, G., Lemoine, M., Vidal-Madjar, A., Désert, J.-M., Lecavelier des Étangs, A., Ferlet, R., Wood, B. E., Linsky, J. L., Kruk, J. W., Chayer, P., Lacour, S., Blair, W. P., Friedman, S. D., Moos, H. W., Sembach, K. R., Sonneborn, G., Oegerle, W. R., & Jenkins, E. B. 2002, *ApJS*, 140, 103
- Hébrard, G. & Moos, H. W. 2003, *ApJ*, 599, 297
- Hébrard, G. 2006, in *Astronomical Society of the Pacific Conference Series*, ed. G. Sonneborn, H. W. Moos, & B.-G. Andersson, 47–+
- Hébrard, G., Tripp, T. M., Chayer, P., Friedman, S. D., Dupuis, J., Sonnentrucker, P., Williger, G. M., & Moos, H. W. 2005, *ApJ*, 635, 1136
- Hoopes, C. G., Sembach, K. R., Hébrard, G., Moos, H. W., & Knauth, D. C. 2003, *ApJ*, 586, 1094
- Howarth, I. D., Siebert, K. W., Hussain, G. A. J., & Prinja, R. K. 1997, *MNRAS*, 284, 265
- Humphreys, R. M. 1978, *ApJS*, 38, 309
- Jenkins, E. B. 1978, *ApJ*, 219, 845
- . 1986, *ApJ*, 304, 739
- Jenkins, E. B., Tripp, T. M., Woźniak, P., Sofia, U. J., & Sonneborn, G. 1999, *ApJ*, 520, 182
- Jura, M. 1974, *ApJ*, 190, L33+
- Jura, M. 1982, in *Advances in Ultraviolet Astronomy*, 54
- Jura, M. & York, D. G. 1978, *ApJ*, 219, 861
- Kirkman, D., Tytler, D., Suzuki, N., O’Meara, J. M., & Lubin, D. 2003, *ApJS*, 149, 1
- Kurucz, R. L. & Peytremann, E. 1975, *SAO Special Report*, 362

- Lemoine, M., Audouze, J., Ben Jaffel, L., Feldman, P., Ferlet, R., Hébrard, G., Jenkins, E. B., Mallouris, C., Moos, W., Sembach, K., Sonneborn, G., Vidal-Madjar, A., & York, D. G. 1999, *New Astronomy*, 4, 231
- Lemoine, M., Vidal-Madjar, A., Hébrard, G., Désert, J.-M., Ferlet, R., Lecavelier des Étangs, A., Howk, J. C., André, M., Blair, W. P., Friedman, S. D., Kruk, J. W., Lacour, S., Moos, H. W., Sembach, K., Chayer, P., Jenkins, E. B., Koester, D., Linsky, J. L., Wood, B. E., Oegerle, W. R., Sonneborn, G., & York, D. G. 2002, *ApJS*, 140, 67
- Linsky, J. L., Diplas, A., Wood, B. E., Brown, A., Ayres, T. R., & Savage, B. D. 1995, *ApJ*, 451, 335
- Linsky, J. L., Draine, B. T., Moos, H. W., Jenkins, E. B., Wood, B. E., Oliveira, C., Blair, W. P., Friedman, S. D., Gry, C., Knauth, D., Kruk, J. W., Lacour, S., Lehner, N., Redfield, S., Shull, J. M., Sonneborn, G., & Williger, G. M. 2006, *ApJ*, 647, 1106
- Maíz-Apellániz, J., Walborn, N. R., Galué, H. Á., & Wei, L. H. 2004, *ApJS*, 151, 103
- Meyer, D. M., Cardelli, J. A., & Sofia, U. J. 1997, *ApJ*, 490, L103
- Meyer, D. M., Jura, M., & Cardelli, J. A. 1998, *ApJ*, 493, 222
- Moos, H. W., Cash, W. C., Cowie, L. L., Davidsen, A. F., Dupree, A. K., Feldman, P. D., Friedman, S. D., Green, J. C., Green, R. F., Gry, C., Hutchings, J. B., Jenkins, E. B., Linsky, J. L., Malina, R. F., Michalitsianos, A. G., Savage, B. D., Shull, J. M., Siegmund, O. H. W., Snow, T. P., Sonneborn, G., Vidal-Madjar, A., Willis, A. J., Woodgate, B. E., York, D. G., Ake, T. B., Andersson, B.-G., Andrews, J. P., Barkhouser, R. H., Bianchi, L., Blair, W. P., Brownsberger, K. R., Cha, A. N., Chayer, P., Conard, S. J., Fullerton, A. W., Gaines, G. A., Grange, R., Gummin, M. A., Hébrard, G., Kriss, G. A., Kruk, J. W., Mark, D., McCarthy, D. K., Morbey, C. L., Murowinski, R., Murphy, E. M., Oegerle, W. R., Ohl, R. G., Oliveira, C., Osterman, S. N., Sahnou, D. J., Saisse, M., Sembach, K. R., Weaver, H. A., Welsh, B. Y., Wilkinson, E., & Zheng, W. 2000, *ApJ*, 538, L1
- Morton, D. C. 1991, *ApJS*, 77, 119
- . 2003, *ApJS*, 149, 205
- Mullan, D. J. & Linsky, J. L. 1999, *ApJ*, 511, 502
- Oliveira, C. M., Dupuis, J., Chayer, P., & Moos, H. W. 2005, *ApJ*, 625, 232

- Oliveira, C. M., Hébrard, G., Howk, J. C., Kruk, J. W., Chayer, P., & Moos, H. W. 2003, *ApJ*, 587, 235
- Oliveira, C. M., Moos, H. W., Chayer, P., & Kruk, J. W. 2006, *ApJ*, 642, 283
- Prochaska, J. X., Tripp, T. M., & Howk, J. C. 2005, *ApJ*, 620, L39
- Prodanović, T. & Fields, B. D. 2003, *ApJ*, 597, 48
- Rachford, B. L., Snow, T. P., Tumlinson, J., Shull, J. M., Blair, W. P., Ferlet, R., Friedman, S. D., Gry, C., Jenkins, E. B., Morton, D. C., Savage, B. D., Sonnentrucker, P., Vidal-Madjar, A., Welty, D. E., & York, D. G. 2002, *ApJ*, 577, 221
- Rogerson, J. B. & York, D. G. 1973, *ApJ*, 186, L95
- Romano, D., Tosi, M., Chiappini, C., & Matteucci, F. 2006, *MNRAS*, 369, 295
- Sahnou, D. J., Moos, H. W., Ake, T. B., Andersen, J., Andersson, B.-G., Andre, M., Artis, D., Berman, A. F., Blair, W. P., Brownsberger, K. R., Calvani, H. M., Chayer, P., Conard, S. J., Feldman, P. D., Friedman, S. D., Fullerton, A. W., Gaines, G. A., Gawne, W. C., Green, J. C., Gummin, M. A., Jennings, T. B., Joyce, J. B., Kaiser, M. E., Kruk, J. W., Lindler, D. J., Massa, D., Murphy, E. M., Oegerle, W. R., Ohl, R. G., Roberts, B. A., Romelfanger, M. L., Roth, K. C., Sankrit, R., Sembach, K. R., Shelton, R. L., Siegmund, O. H. W., Silva, C. J., Sonneborn, G., Vaclavik, S. R., Weaver, H. A., & Wilkinson, E. 2000, *ApJ*, 538, L7
- Savage, B. D., Bohlin, R. C., Drake, J. F., & Budich, W. 1977, *ApJ*, 216, 291
- Schectman, R. M., Federman, S. R., Beideck, D. J., & Ellis, D. J. 1993, *ApJ*, 406, 735
- Sembach, K. R., Wakker, B. P., Tripp, T. M., Richter, P., Kruk, J. W., Blair, W. P., Moos, H. W., Savage, B. D., Shull, J. M., York, D. G., Sonneborn, G., Hébrard, G., Ferlet, R., Vidal-Madjar, A., Friedman, S. D., & Jenkins, E. B. 2004, *ApJS*, 150, 387
- Sfeir, D. M., Lallement, R., Crifo, F., & Welsh, B. Y. 1999, *A&A*, 346, 785
- Shull, J. M. & van Steenberg, M. 1982, *ApJS*, 48, 95
- Shull, J. M. & van Steenberg, M. E. 1985, *ApJ*, 294, 599
- Sonneborn, G., Tripp, T. M., Ferlet, R., Jenkins, E. B., Sofia, U. J., Vidal-Madjar, A., & Woźniak, P. . R. 2000, *ApJ*, 545, 277

Spergel, D. N., Bean, R., Dore', O., Nolta, M. R., Bennett, C. L., Hinshaw, G., Jarosik, N., Komatsu, E., Page, L., Peiris, H. V., Verde, L., Barnes, C., Halpern, M., Hill, R. S., Kogut, A., Limon, M., Meyer, S. S., Odegard, N., Tucker, G. S., Weiland, J. L., Wollack, E., & Wright, E. L. 2006, ArXiv Astrophysics e-prints

Williger, G. M., Oliveira, C., Hébrard, G., Dupuis, J., Dreizler, S., & Moos, H. W. 2005, ApJ, 625, 210

Wood, B. E., Linsky, J. L., Hébrard, G., Williger, G. M., Moos, H. W., & Blair, W. P. 2004, ApJ, 609, 838

York, D. G. 1983, ApJ, 264, 172

Table 1. Stellar Properties

Star	$d$ (pc)	$l$ ( $^{\circ}$ )	$b$ ( $^{\circ}$ )	Sp. Type	$v_{\sin i}$ (km s $^{-1}$ )	$E_{B-V}$
HD 41161	1253	164.97	+12.89	O8.0 V	300	0.20
HD 53975	1318	225.68	−2.32	O7.5 V	163	0.22

Note. — All stellar properties are from Diplas & Savage (1994a) except for  $v_{\sin i}$  which are from Howarth et al. (1997). Distances are based on photometry and are probably accurate within  $\sim 25\%$ .

Table 2. Log of *FUSE* observations

Star	Program ID	Aperture	Mode	Time (s)	Date	CalFUSE
HD 41161	P1021001	LWRS	HIST	58	2001 Feb 20	3.0.7
...	P1021002 <sup>a</sup>	MDRS	HIST	6520	2003 Sept 25	3.0.8
HD 53975	P3032301 <sup>a</sup>	MDRS	HIST	482	2004 Feb 04	3.0.7

<sup>a</sup>Only SiC data obtained during these observations.



Table 3. Atomic data and equivalent widths (mÅ) for the lines used in the analyses<sup>a</sup>

Species	Wavelength (Å)	Log $f\lambda$	HD 41161	HD 53975
DI	916.1785	−0.28	(A, P)	(A, P)
...	916.9311	−0.18	...	(P)
...	917.8797	−0.07	(P)	...
...	919.1013	0.04	...	(P)
...	920.713	0.17	...	(A, P)
CI	945.1910	2.16	89.59 ± 2.55 (A)	51.37 ± 4.30 (A)
CIII	977.0200	2.87	222.90 ± 6.22 (A)	311.13 ± 17.61 (A)
NI	951.0792	−0.79	67.53 ± 2.42 (C, P)	49.96 ± 4.01 (C, P)
...	951.2948	−1.66	18.52 ± 1.95 (A, C, P)	24.68 ± 3.76 (C, P)
...	953.4152	1.09	126.05 ± 2.37 (C)	144.00 ± 3.45 (C)
...	953.6549	1.37	132.32 ± 2.60 (C)	147.30 ± 3.41 (C)
...	959.4937	−1.30	28.89 ± 1.26 (C, P)	22.55 ± 2.39 (A, C, P)
...	960.2014	−1.95	...	(P)
...	963.9903	1.08	...	154.30 ± 5.03 (C)
...	964.6256	0.88	...	128.36 ± 8.29 (C)
...	1134.1653	1.22	158.26 ± 4.92 (C)	...
...	1134.4149	1.51	162.92 ± 5.15 (C)	...
...	1134.9803	1.67	180.55 ± 6.35 (C)	...
NII	1083.994	2.10	170.00 ± 4.94 (A)	244.55 ± 9.95 (A)
OI	974.070	−1.82	(P)	(P)
OVI	1031.9261	2.13	...	91.16 ± 12.84 (P)
...	1037.6167	1.83	...	42.92 ± 7.22 (A, P)
Mg II	946.7033	−0.17	...	(P)
...	946.7694	−0.48	...	(P)
P II	961.0412	2.53	74.90 ± 2.23 (A)	88.23 ± 4.74 (A)
S III	1012.4950	1.65	...	86.38 ± 10.13 (P)
Cl I	1088.0589	1.95	44.55 ± 1.97 (A)	14.16 ± 3.46 (A)
Cl II	1071.0358	1.21	16.16 ± 0.96 (A)	...
Ar I	1066.6599	1.86	114.17 ± 3.03 (A)	158.12 ± 7.86 (A)
Ar II	919.7810	0.91	...	(P)
Fe II	926.8969	0.72	...	19.76 ± 2.06 (C, P)

Table 3—Continued

Species	Wavelength (Å)	Log $f\lambda$	HD 41161	HD 53975
...	1055.2617	0.90	$46.34 \pm 1.31$ (C, P)	$46.33 \pm 2.44$ (A, C, P)
...	1062.1517	0.49	$17.59 \pm 2.17$ (C, P)	...
...	1063.9718	0.60	$20.41 \pm 2.19$ (C)	$19.18 \pm 3.70$ (A, C)
...	1081.8748	1.13	$88.26 \pm 2.36$ (C)	$61.79 \pm 3.59$ (C)
...	1083.4204	0.48	$27.75 \pm 2.22$ (C, P)	...
...	1096.8770	1.55	$93.16 \pm 3.03$ (C)	...
...	1112.0480	0.84	$34.34 \pm 3.78$ (C)	...
...	1121.9749	1.36	$83.15 \pm 5.79$ (C)	...
...	1125.448	1.26	$84.07 \pm 4.35$ (C)	...
...	1127.0984	0.50	$25.86 \pm 5.16$ (A, C)	...
...	1133.6654	0.80	$50.57 \pm 3.73$ (A, C, P)	...
...	1142.3656	0.68	$45.39 \pm 4.79$ (C, P)	...
...	1143.2260	1.31	$80.79 \pm 4.64$ (C,P)	...
...	1144.938	2.08	$122.30 \pm 5.36$ (C)	...

<sup>a</sup>A, C, and P indicate which methods were used with each transition and stand for apparent optical depth, curve-of-growth, and profile fitting, respectively.

Table 4. Atomic Column Densities (Log) for HD 41161

Species	AOD	COG	PF	Adopted
HI	...	...	...	$21.00 \pm 0.09^a$
DI	$16.37 \pm 0.04$ ( $\lambda 916.18$ )	...	$16.43 \pm 0.03$	$16.40 \pm 0.05$
NI	$17.06 \pm 0.04$ ( $\lambda 951.29$ )	$17.00 \pm \begin{smallmatrix} 0.04 \\ 0.03 \end{smallmatrix}$	$16.94 \pm 0.01$	$17.00 \pm 0.06$
OI	...	...	$18.04 \pm 0.05$	$18.04 \pm 0.05$
FeII	$14.96 \pm \begin{smallmatrix} 0.08 \\ 0.10 \end{smallmatrix}$ ( $\lambda 1127$ )	$15.02 \pm 0.06$	$14.94 \pm 0.03$	$14.98 \pm 0.06$
ClI	$13.72 \pm 0.04$ ( $\lambda 1088$ )	...	...	$13.72 \pm 0.04$
CI	$\geq 14.13$ ( $\lambda 945$ )	...	...	$\geq 14.13$
CIII	$\geq 14.04$ ( $\lambda 977$ )	...	...	$\geq 14.04$
NII	$\geq 14.52$ ( $\lambda 1083$ )	...	...	$\geq 14.52$
P II	$\geq 13.63$ ( $\lambda 961$ )	...	...	$\geq 13.63$
ClII	$\geq 14.02$ ( $\lambda 1071$ )	...	...	$\geq 14.02$
ArI	$\geq 14.52$ ( $\lambda 1066$ )	...	...	$\geq 14.52$

<sup>a</sup>See §2.1.

Note. — All uncertainties are  $1\sigma$ .

Table 5. Molecular Column Densities (Log)

Species	HD 41161	HD 53975
HD ( $J = 0$ )	$14.57 \pm 0.08$	$13.42 \pm 0.10$
H <sub>2</sub> ( $J = 0$ )	$19.63 \pm 0.06$	$18.79 \pm 0.05$
... ( $J = 1$ )	$19.72 \pm 0.06$	$18.95 \pm 0.05$
... ( $J = 2$ )	$17.97 \pm 0.10$	17.8:
... ( $J = 3$ )	$17.40 \pm 0.10$	17.7:
... ( $J = 4$ )	$14.95 \pm 0.08$	$14.33 \pm 0.05$
... ( $J = 5$ )	$14.34 \pm 0.05$	$13.80 \pm 0.05$
$N(\text{H}_2)$	$19.98 \pm \begin{smallmatrix} 0.08 \\ 0.09 \end{smallmatrix}$	$19.18 \pm 0.04$
$N(\text{H})$	$21.08 \pm 0.08$	$21.14 \pm 0.06$

Note. — All uncertainties are  $1\sigma$ .

Table 6. Atomic Column Densities (Log) for HD 53975

Species	AOD	COG	PF	Adopted
HI	...	...	...	$21.13 \pm 0.06^a$
DI	$16.11 \pm 0.03$ ( $\lambda 920.7$ )	...	$16.20 \pm 0.02$	$16.15 \pm 0.07$
NI	$16.73 \pm 0.05$ ( $\lambda 959.49$ )	$16.89 \pm \begin{smallmatrix} 0.10 \\ 0.07 \end{smallmatrix}$	$16.84 \pm 0.05$	$16.80 \pm 0.08$
OI	...	...	$17.87 \pm 0.08$	$17.87 \pm 0.08$
OVI	$13.97 \pm 0.07$ ( $\lambda 1031$ )	...	$13.96 \pm 0.03$	$13.96 \pm 0.05$
FeII	$14.80 \pm \begin{smallmatrix} 0.07 \\ 0.08 \end{smallmatrix}$ ( $\lambda 1063.9$ )	$14.87 \pm \begin{smallmatrix} 0.08 \\ 0.11 \end{smallmatrix}$	$14.84 \pm \begin{smallmatrix} 0.02 \\ 0.03 \end{smallmatrix}$	$14.84 \pm 0.05$
MgII	...	...	$16.10 \pm 0.05$	$16.10 \pm 0.05$
ClI	$13.53 \pm 0.10$ ( $\lambda 1088$ )	...	...	$13.53 \pm 0.10$
CI	$\geq 13.73$ ( $\lambda 945$ )	...	...	$\geq 13.73$
CIII	$\geq 14.22$ ( $\lambda 977$ )	...	...	$\geq 14.22$
NII	$\geq 14.73$ ( $\lambda 1083$ )	...	...	$\geq 14.73$
P II	$\geq 13.62$ ( $\lambda 961$ )	...	...	$\geq 13.62$
SIII	$\geq 14.54$ ( $\lambda 1012$ )	...	...	$\geq 14.54$
Ar I	$\geq 14.67$ ( $\lambda 1066$ )	...	...	$\geq 14.67$

<sup>a</sup>See § 2.2.

Note. — All uncertainties are  $1\sigma$ .

Table 7. Ratios of Column Densities

Ratio	HD 41161	HD 53975
$(\text{D}/\text{H}) \times 10^5$	$2.14 \pm \begin{smallmatrix} 0.51 \\ 0.43 \end{smallmatrix}$	$1.02 \pm \begin{smallmatrix} 0.23 \\ 0.20 \end{smallmatrix}$
$(\text{N}/\text{H}) \times 10^5$	$8.32 \pm \begin{smallmatrix} 2.09 \\ 1.76 \end{smallmatrix}$	$5.07 \pm \begin{smallmatrix} 1.45 \\ 1.21 \end{smallmatrix}$
$(\text{O}/\text{H}) \times 10^4$	$9.12 \pm \begin{smallmatrix} 2.15 \\ 1.83 \end{smallmatrix}$	$5.37 \pm \begin{smallmatrix} 1.35 \\ 1.14 \end{smallmatrix}$
$(\text{Fe}/\text{H}) \times 10^6$	$0.79 \pm \begin{smallmatrix} 0.20 \\ 0.17 \end{smallmatrix}$	$0.50 \pm \begin{smallmatrix} 0.10 \\ 0.08 \end{smallmatrix}$
$(\text{D}/\text{O}) \times 10^2$	$2.29 \pm \begin{smallmatrix} 0.40 \\ 0.35 \end{smallmatrix}$	$1.91 \pm \begin{smallmatrix} 0.51 \\ 0.43 \end{smallmatrix}$
O/N	$10.96 \pm \begin{smallmatrix} 2.10 \\ 1.85 \end{smallmatrix}$	$11.74 \pm \begin{smallmatrix} 3.36 \\ 2.80 \end{smallmatrix}$
$(\text{HD}/\text{H}_2) \times 10^6$	$3.89 \pm \begin{smallmatrix} 1.11 \\ 0.93 \end{smallmatrix}$	$1.74 \pm \begin{smallmatrix} 0.48 \\ 0.39 \end{smallmatrix}$
$f_{\text{H}_2}$ (%)	$16.0 \pm \begin{smallmatrix} 4.0 \\ 3.4 \end{smallmatrix}$	$2.2 \pm \begin{smallmatrix} 0.4 \\ 0.3 \end{smallmatrix}$
$\langle n_{\text{H}} \rangle$ ( $\text{cm}^{-3}$ )	0.31	0.34

Note. — All uncertainties are  $1\sigma$  and  $\text{D}/\text{H} = [N(\text{D I}) + N(\text{HD})]/[N(\text{H I}) + 2 \times N(\text{H}_2) + N(\text{HD})]$ .

Table 8. Equivalent Widths and Atomic Data for CII along the HD 41161 Sightline

Wavelength (Å)	$f$	Ref.	$W_\lambda$ (mÅ)	$f_{\text{pred.}}^{\text{a}}$
969.9195	$1.73 \times 10^{-2}$	1	$4.38 \pm 0.93$	$(1.0 \pm 0.2) \times 10^{-2}$
984.2865 <sup>b</sup>	$2.44 \times 10^{-2}$	1, 4	$13.18 \pm 1.95$	$(2.9 \pm 0.5) \times 10^{-2}$
1004.6776	$1.58 \times 10^{-1}$	1, 4	$28.63 \pm 1.39$	$(6.1 \pm 0.7) \times 10^{-2}$
1022.0478	$1.22 \times 10^{-2}$	1	$9.35 \pm 1.24$	$(1.9 \pm 0.3) \times 10^{-2}$
1027.3386	$6.58 \times 10^{-3}$	1	$12.08 \pm 2.97$	$(2.5 \pm 0.7) \times 10^{-2}$
1031.5070	$1.51 \times 10^{-1}$	1, 5	$10.23 \pm 3.42$	$(2.1 \pm 0.7) \times 10^{-2}$
1085.3035	$5.81 \times 10^{-4}$	2, 5	$12.32 \pm 2.16$	$(2.2 \pm 0.5) \times 10^{-2}$
1088.0589	$(8.1 \pm 0.7) \times 10^{-2}$	3, 5	$44.55 \pm 1.97$	...
1094.7686	$1.66 \times 10^{-2}$	2, 5	$40.21 \pm 3.04$	$(7.2 \pm 0.9) \times 10^{-2}$
1347.2396	$(1.53 \pm 0.11) \times 10^{-1}$	3, 5	$104.9 \pm 17.4$	...
978.5932	$1.85 \times 10^{-1}$	1, 5	<4.5	< $1.0 \times 10^{-2}$
1043.9860	$1.81 \times 10^{-2}$	1, 5	<2.7	< $5.3 \times 10^{-3}$
1079.8821	$6.98 \times 10^{-3}$	2, 5	<4.1	< $7.5 \times 10^{-3}$
1099.5230	$1.14 \times 10^{-2}$	2, 5	<10.0	< $1.8 \times 10^{-2}$
1101.9361	$1.13 \times 10^{-2}$	2, 5	<5.1	< $9.1 \times 10^{-3}$

<sup>a</sup>See § 7 for a discussion of how  $f_{\text{pred.}}$  is calculated.

<sup>b</sup>Possibly blended with the  $\lambda 984.323$  transition.

Note. — For the last six transitions we quote  $1\sigma$  upper limits on the equivalent widths.

References. — References 1–3 refer to the original papers. References 4 and 5 are compilations of atomic data. (1) Kurucz & Peytremann (1975), (2) Biemont et al. (1994), (3) Schectman et al. (1993), (4) Morton (1991), (5) Morton (2003).

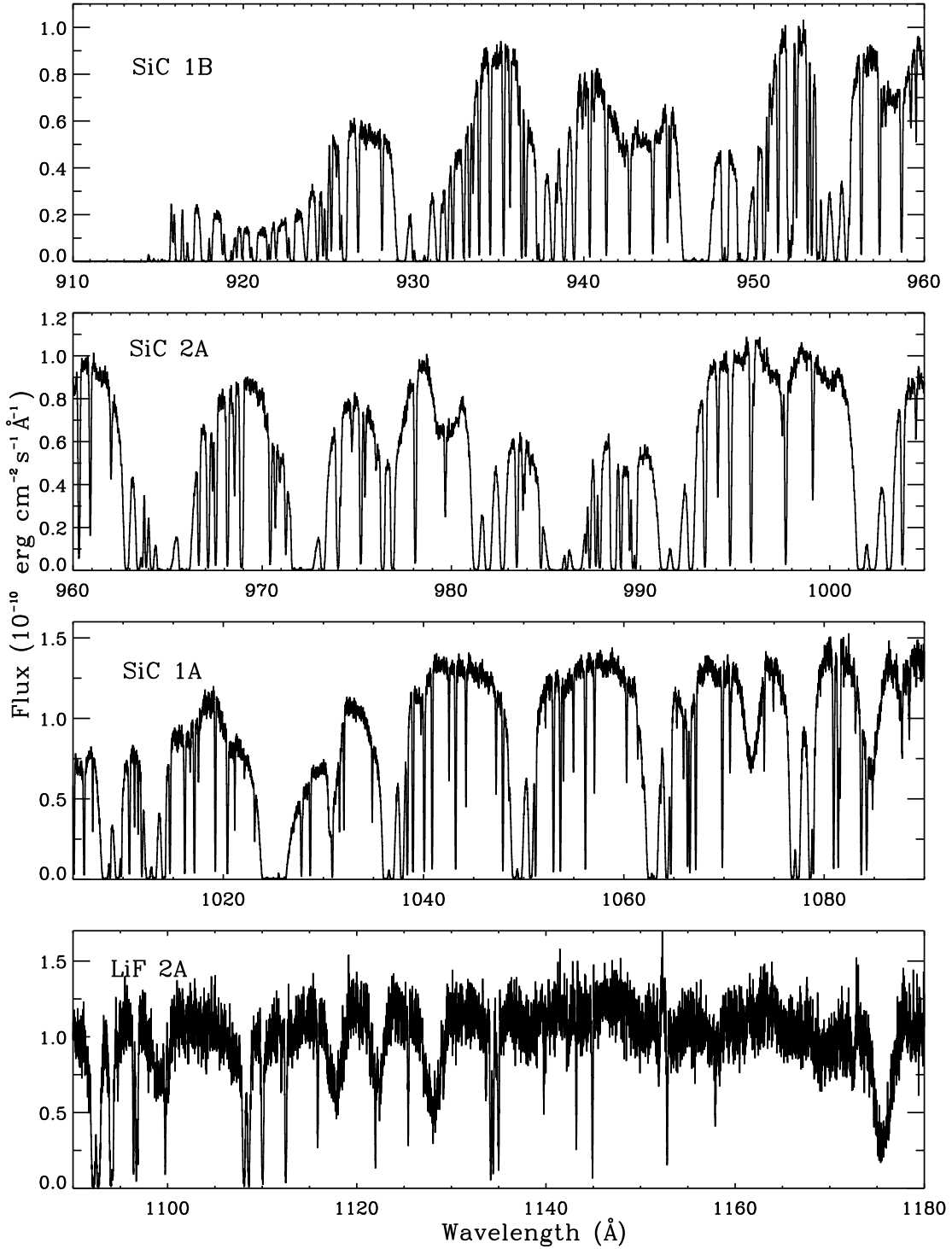


Fig. 1.— *FUSE* spectrum of HD 41161. The *FUSE* channel used for each panel is indicated at the top, in the left. The SiC data displayed is from the MDRS observation, the LiF one from the LWRS observation (no LiF data obtained in the MDRS observation; see Table 2).



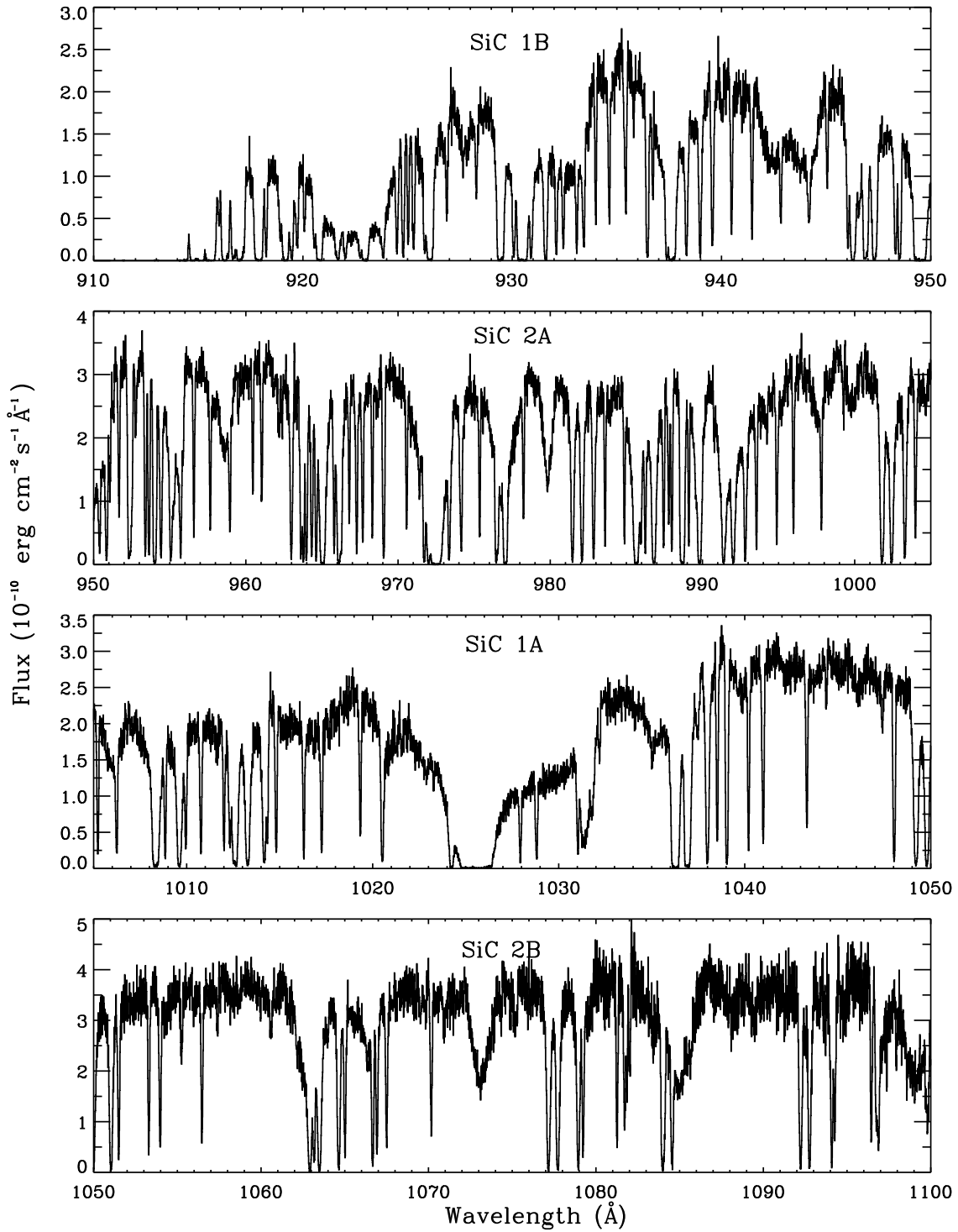


Fig. 2.— *FUSE* spectrum of HD 53975. The *FUSE* channel used for each panel is indicated at the top, in the center. No LiF data was obtained for this target.

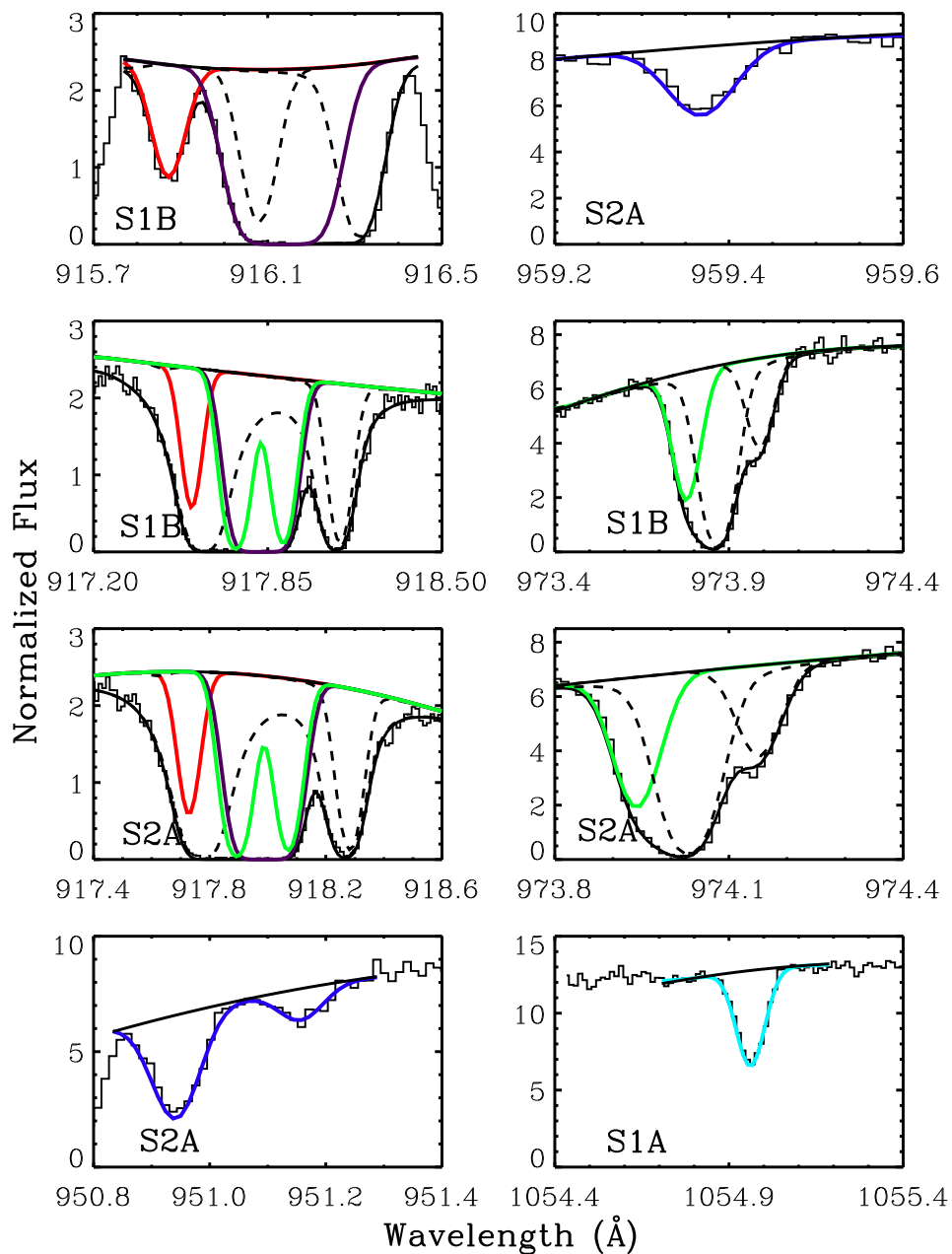


Fig. 3.— Fits to some of the lines used to determine column densities along the HD 41161 sightline (convolved with the instrument LSF). Absorption by HI is represented by magenta, DI by red, NI by dark blue, OI by green, and Fe II by cyan. Absorption by H<sub>2</sub> is represented by black dashed lines. See § 4.1 for discussion.

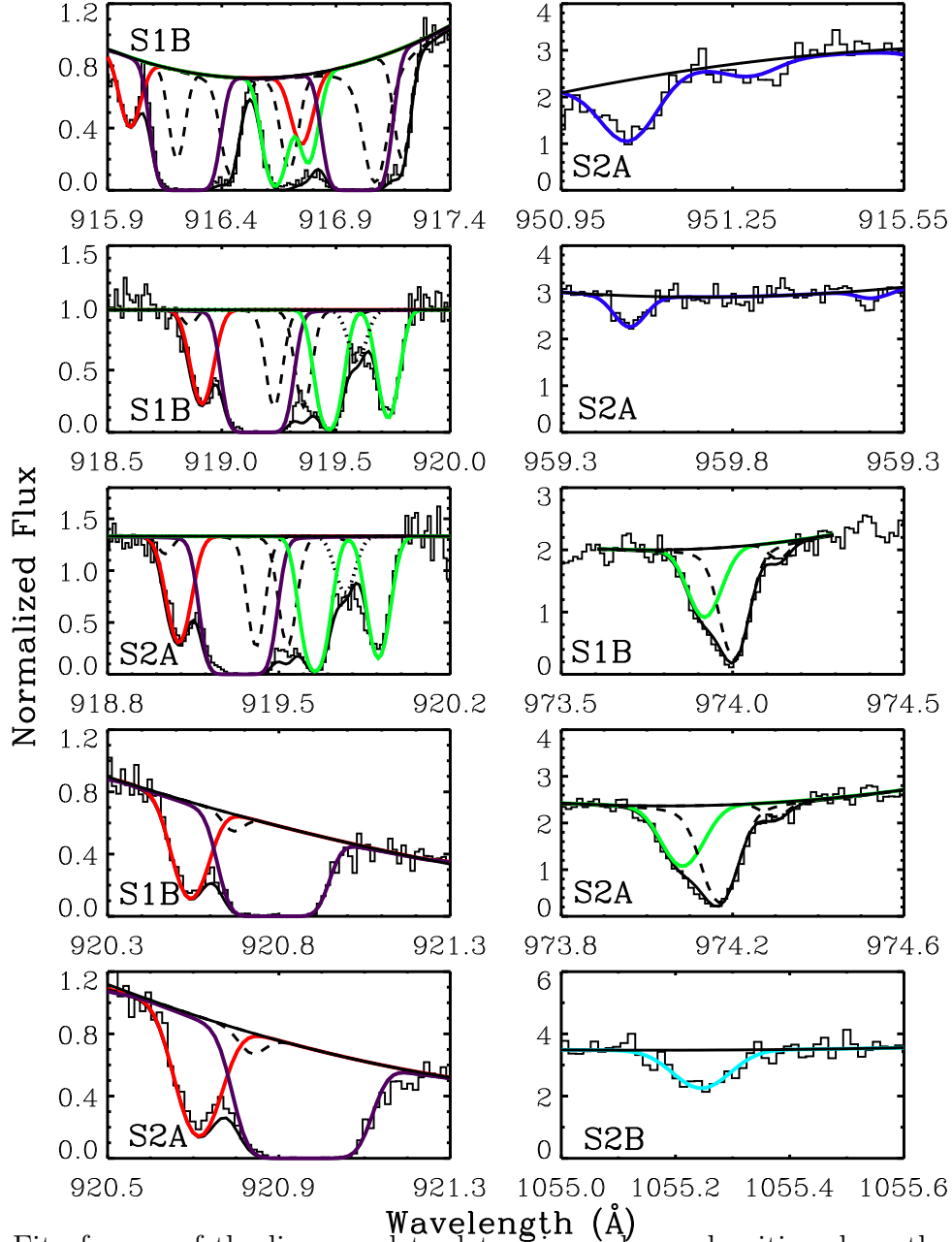


Fig. 4.— Fit of some of the lines used to determine column densities along the HD 53975 sightline (convolved with the instrument LSF). Colors are the same as in Figure 3. Absorption by Ar II is represented by a black dotted line. See § 4.3 for discussion.

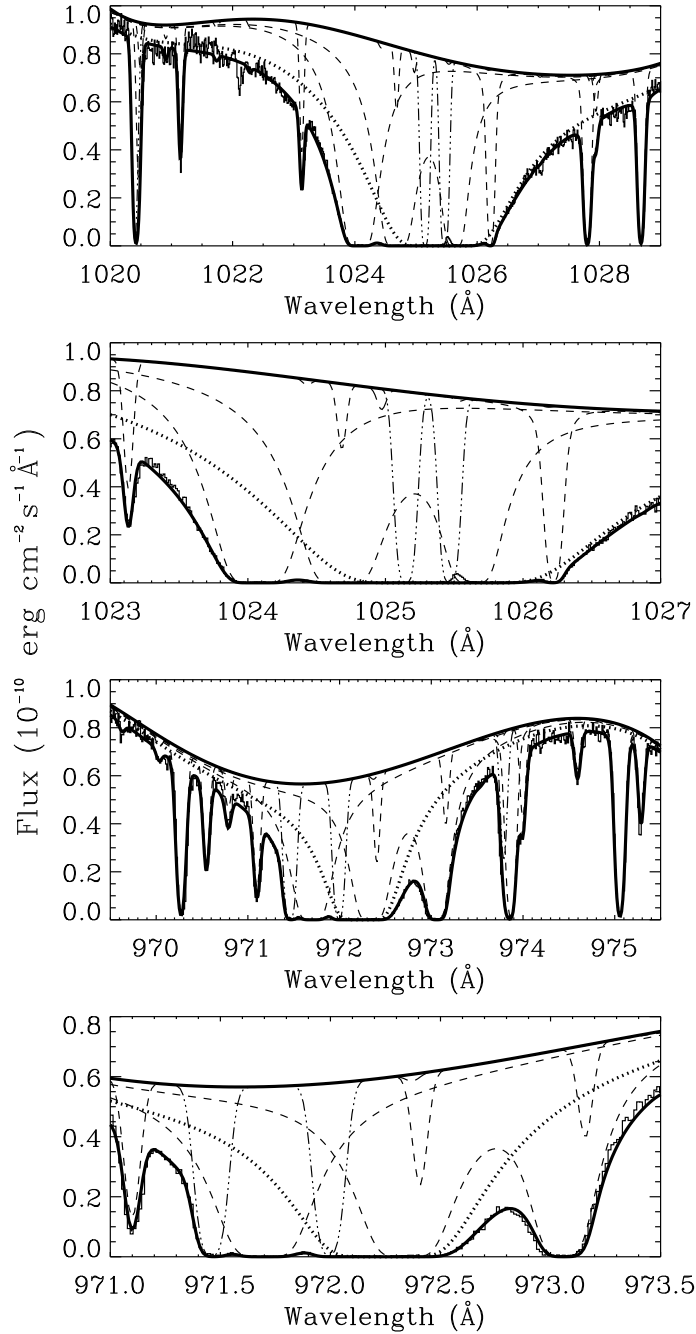


Fig. 5.— Fit to HI Ly $\beta$  (first and second panels) and Ly $\gamma$  (third and fourth panels) transitions along the HD 41161 sightline, yielding  $\log N(\text{HI}) = 21.13 \pm_{0.05}^{0.04}$ , in agreement with the value adopted in §2.1. The cores of the Ly $\beta$  and Ly $\gamma$  lines are presented in more detail in the second and fourth panels, respectively. H<sub>2</sub> is represented by dashed lines, O I, Si II, D I, and Fe II by dash-dot-dot. HI is represented by a thick dotted line. The two top panels are from S1A MDRS, while the bottom two are from S2B MDRS. The small bump near 1025.5 Å is due to airglow emission, and does not affect our measurements. See §5.1 for discussion.

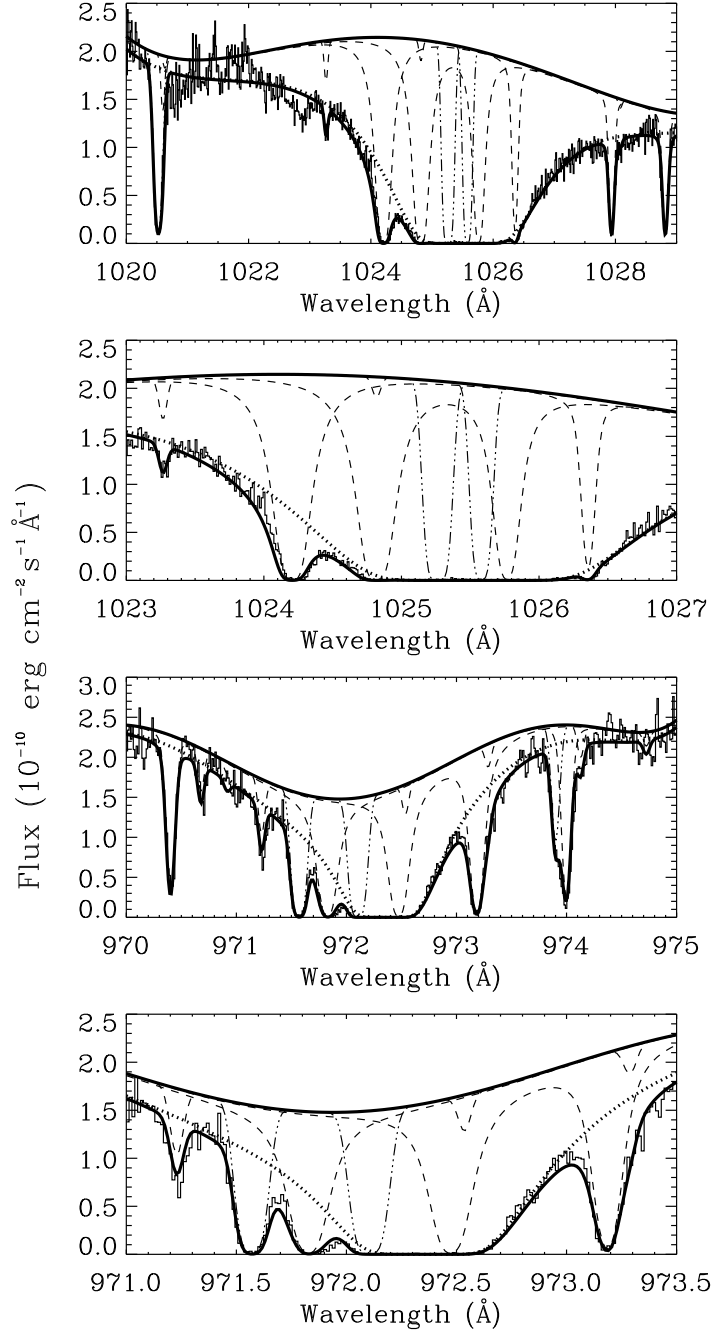


Fig. 6.— Same as Fig. 5 but for the HD 53975 sightline, yielding  $\log N(\text{HI}) = 21.19 \pm 0.01$ , in agreement with the value adopted in §2.2. The two top panels are from S1B, while the bottom two are from S1A. See §5.2 for discussion.

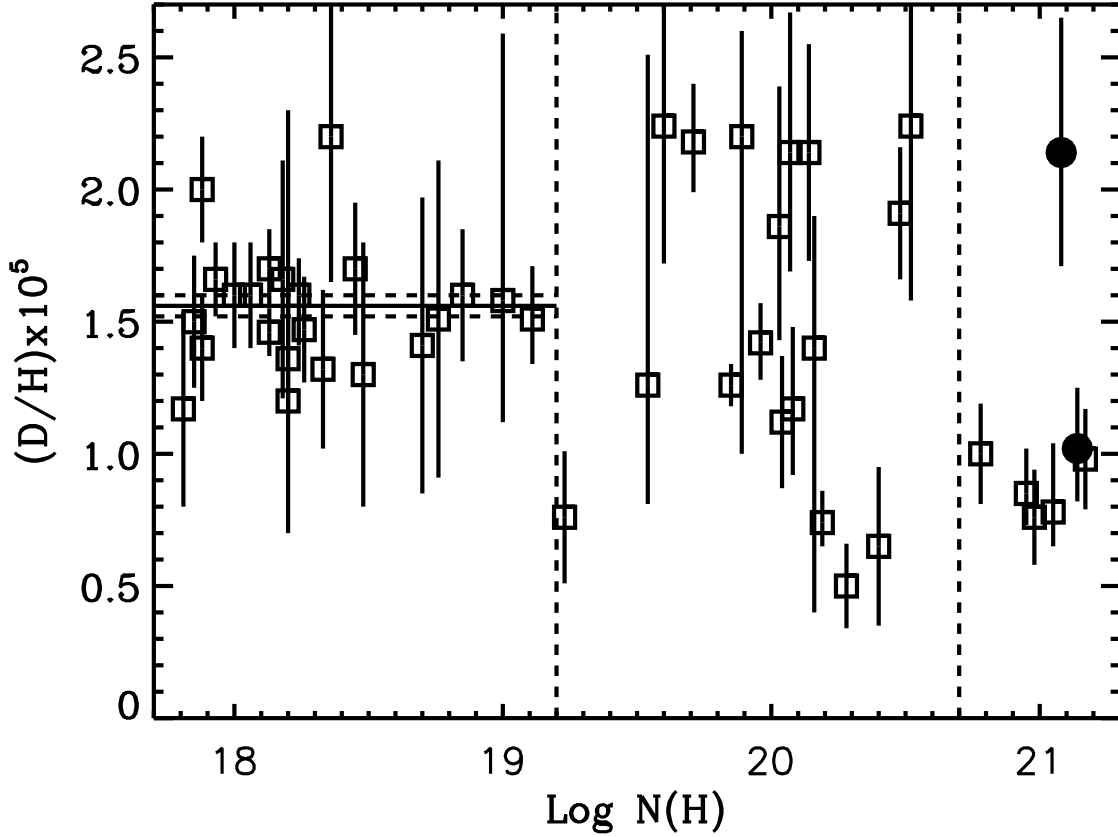


Fig. 7.—  $D/H$  as a function of  $\log N(\text{H})$ . Open squares represent ratios from the literature and from Oliveira et al. (2006) (where references to all the individual ratios presented can be found), filled circles the two new ratios derived in this work. Dashed and solid horizontal lines mark the Local Bubble  $D/H$  ratio  $(1.56 \pm 0.04) \times 10^{-5}$  derived from a compilation of measurements by Wood et al. (2004). Dashed vertical lines mark  $\log N(\text{H}) = 19.2$  corresponding to the edge of the Local Bubble, and  $\log N(\text{H}) = 20.7$  after which Wood et al. (2004) and Linsky et al. (2006) proposed that  $D/H$  was low and constant.

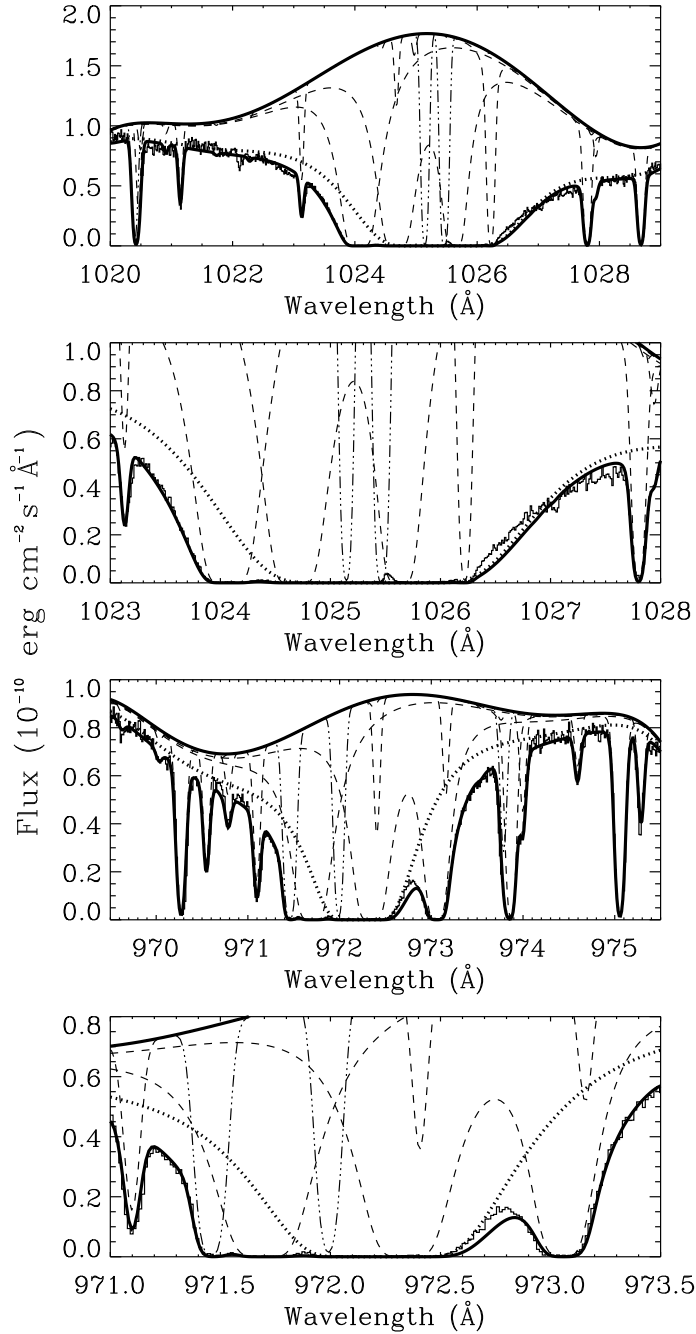


Fig. 8.— Forced fit to HI Ly $\beta$  (first and second panels) and Ly $\gamma$  (third and fourth panels) transitions along the HD 41161 sightline, with  $\log N(\text{HI}) = 21.44$ , required to bring D/H along this sightline to agree with D/H for other 5 sightlines with similar  $N(\text{H})$ . Dashed lines represent H<sub>2</sub>, dash-dot-dot O I, Si II, D I, and Fe II. HI is represented by a thick dotted line. The two top panels are from S1A MDRS, while the bottom two are from S2B MDRS. The cores of the Ly $\beta$  and Ly $\gamma$  transitions, presented in more detail in the second and fourth panels, show that  $\log N(\text{HI}) = 21.44$  clearly overestimates the true HI absorption. See §6.1.1 for discussion.

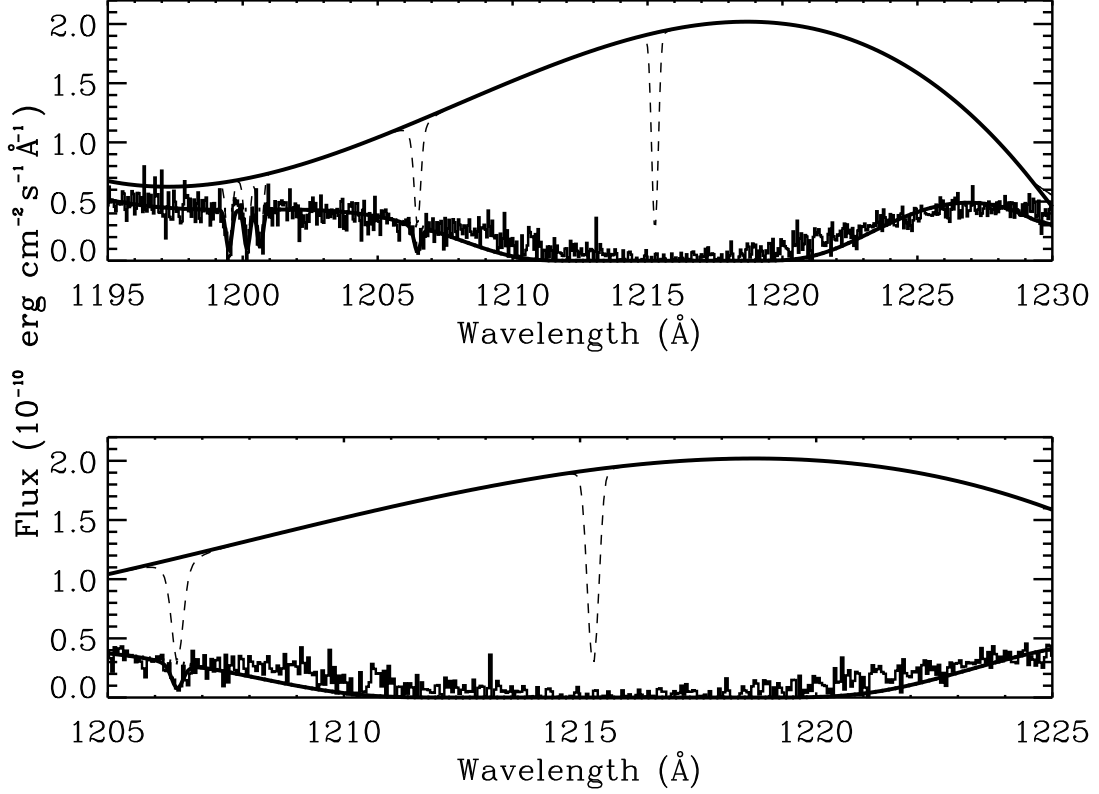


Fig. 9.— Forced fit to the HI Ly $\alpha$  transition along the HD 41161 sightline, with  $\log N(\text{HI}) = 21.44$ , required to bring D/H along this sightline to agree with D/H for other 5 sightlines with similar  $N(\text{H})$ . Dashed lines represent N I, Si III, and D I. The global fit, including HI, as well as the continuum, are represented by thick solid lines. The core of the Ly $\alpha$  transition, presented in more detail in the second panel clearly shows that  $\log N(\text{HI}) = 21.44$  clearly overestimates the true HI absorption. See §6.1.1 for discussion.



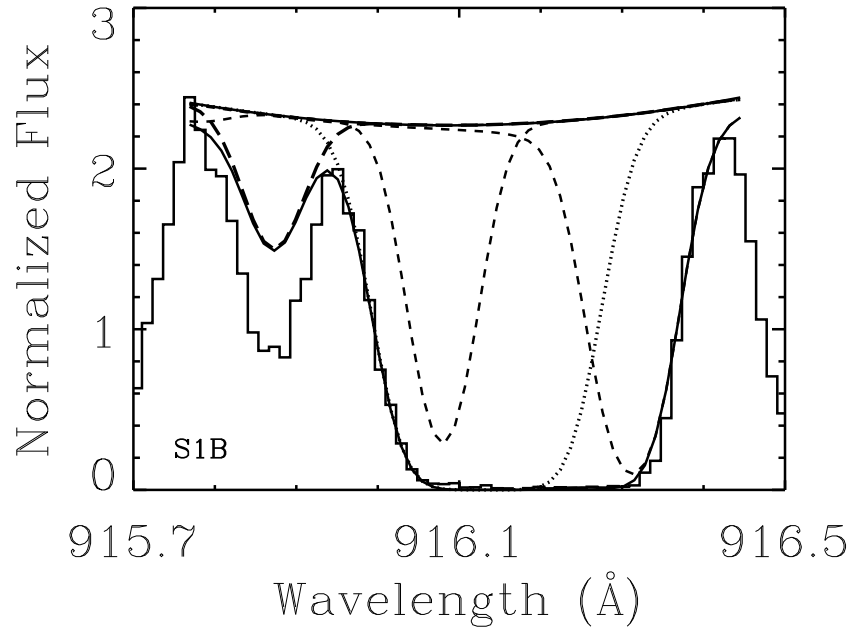


Fig. 10.—  $\log N(\text{DI}) = 16.00$ , required to lower D/H along the HD 41161 sightline, superimposed on DI  $\lambda 916.2$ . Absorption is represented by short-dashed lines for HI, long-dashed lines for DI, and dotted lines for  $\text{H}_2$ . The overall fit and continuum are represented by solid lines. This figure shows that  $\log N(\text{DI}) = 16.00$  clearly underestimates the true DI absorption. Compare this figure to the corresponding panel in Fig. 3 where we derive  $\log N(\text{DI}) = 16.43 \pm 0.03$ . See §6.1.1 for discussion.

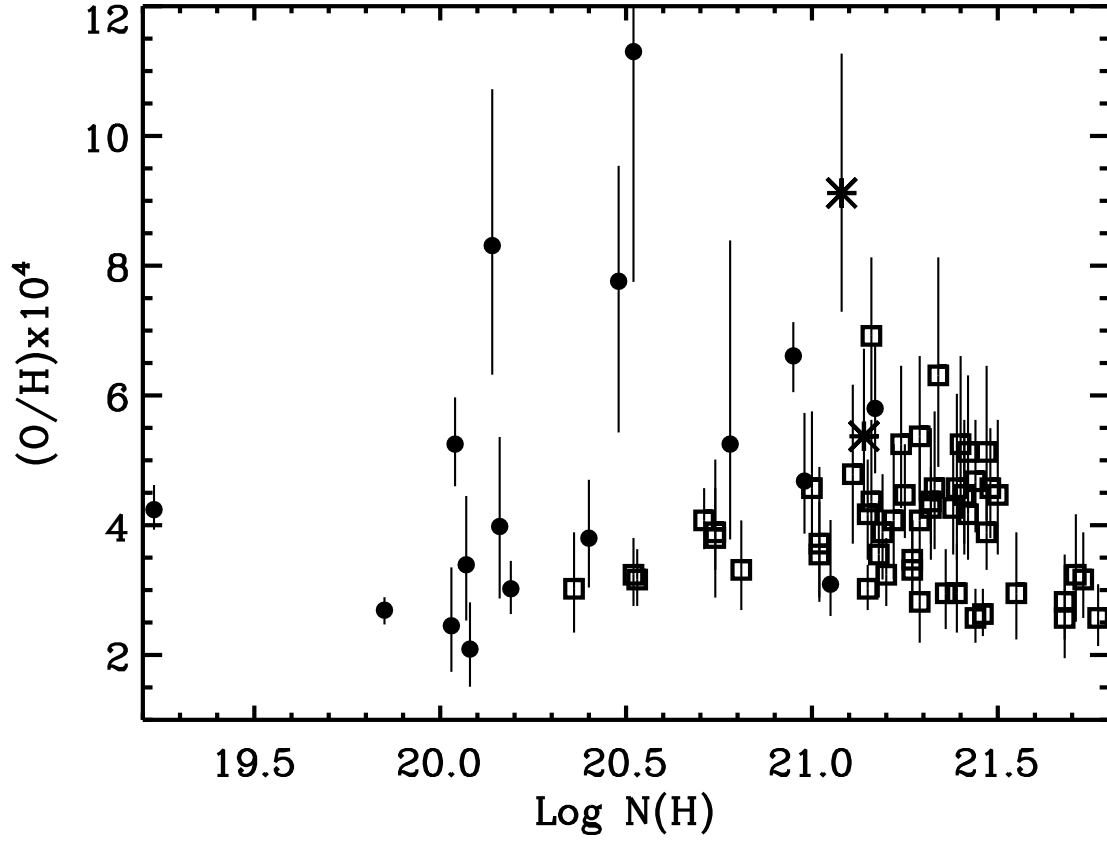


Fig. 11.—  $\text{O}/\text{H}$  as a function of  $\text{Log } N(\text{H})$ . Filled circles correspond to *FUSE* based measurements from the literature (see for e.g. Oliveira et al. 2006, for a compilation of these values). The two new values derived here are represented by asterisks and open squares represent *HST* based measurements from Cartledge et al. (2004).